

# Preclinical pharmacokinetics and disposition of a novel selective VEGFR inhibitor Fruquintinib (HMPL-013) and the prediction of its human pharmacokinetics

Yi Gu · Jian Wang · Ke Li · Li Zhang · Hongcan Ren ·  
Lixia Guo · Yang Sai · Weihang Zhang · Weiguo Su

Received: 14 February 2014 / Accepted: 22 April 2014 / Published online: 11 May 2014  
© Springer-Verlag Berlin Heidelberg 2014

## Abstract

**Purpose** This study evaluated the preclinical pharmacokinetics (PK) and disposition of Fruquintinib (HMPL-013), a small molecule vascular endothelial growth factor receptors inhibitor.

**Methods** In vitro and in vivo PK/ADME assays were conducted. Allometry and PK modeling/simulation were conducted to predict human PK parameters and the time course profiles.

**Results** HMPL-013 has high permeability without efflux. It shows moderate oral bioavailability of 42–53 % and  $T_{\max} < 4$  h in mouse, rat, dog and monkey, with exposure-dose linearity proved in rats and dogs. No significant food effect is on dog PK. HMPL-013 has moderately high tissue distribution. It majorly distributes in gastrointestinal tract, liver, kidney, adrenal and adipose. The plasma protein binding fraction is 88–95 % in mouse, rat, dog and human, invariable up to 10  $\mu$ M. The in vivo clearance of HMPL-013 is low, consistent with the in vitro scaling. Three major oxidative metabolites were identified in liver microsomes of mouse, rat, dog, monkey and human. Dog is mostly

similar to human regarding in vitro metabolism. Demethylation, hydroxylation and sequential glucuronidation are the major in vivo metabolic reactions. Direct urinary and biliary excretion of HMPL-013 is negligible. Metabolizing to M1 (demethylation), sequentially glucuronidating, followed by biliary excretion, and to a less extent, by urinary excretion, are important elimination pathways for HMPL-013 in rats. HMPL-013 has low risk of drug–drug interaction. It is predicted to have favorable human PK properties and low efficacious dose.

**Conclusion** HMPL-013 demonstrates good preclinical PK and enables successful human PK and dose projection. It is valuable for further clinical development.

**Keywords** Fruquintinib · HMPL-013 · Pharmacokinetics · Disposition · Allometric scaling · Modeling

## Abbreviations

VEGF	Vascular endothelial growth factor
VEGFR	Vascular endothelial growth factor receptors
TKI	Tyrosine kinase inhibitors
PK	Pharmacokinetics
ADME	Absorption, distribution, metabolism and excretion
RED	Rapid equilibrium dialysis
CYP	Cytochrome P450
API	Active pharmaceutical ingredient
AUC <sub>inf</sub>	Area under the concentration–time curve from time zero to infinity
$C_{\max}$	Maximal concentration
$T_{\max}$	Time to reach the maximal concentration
MID	Metabolite identification
IS	Internal standard
$t_{1/2}$	Half-lives

This work has been partially presented by poster in the 17th ISSX north American regional meeting (Atlanta, GA, 2011), Abstract #P103.

Y. Gu · J. Wang · K. Li · L. Zhang · H. Ren · L. Guo ·  
Y. Sai (✉) · W. Zhang · W. Su  
Department of Clinical Pharmacology and DMPK, Hutchison  
MediPharma Limited, Building 4, 720 Cailun Road, Zhang-Jiang  
Hi-Tech Park, Shanghai 201203, China  
e-mail: yangs@hmpglobal.com

## Present Address:

K. Li  
Preclinical Development and Safety Asia Pacific,  
Janssen Research and Development, Shanghai, China

$CL_R$	Renal clearance
$CL_B$	Biliary clearance
$CL$	Plasma total clearance
$V_z$	Volume of distribution at the terminal phase
BW	Body weight
RoE	Rule of exponents
FIH	First-in-human
PD	Pharmacodynamic
$CL_{\text{hep,pred}}$	Predicted hepatic clearance
$CL_{\text{int}}$	In vitro intrinsic clearance
BDC	Bile duct cannulated
MLP	Maximal life span potential
Tlag	Lag time
$K_a$	Absorption rate constant
DDI	Drug–drug interaction
$f_e$	Fraction excreted
$f_m$	Fraction metabolized
GFR	Glomerular filtration rate
PBPK	Physiological-based PK

## Introduction

Anti-angiogenic strategies targeting the developing tumor neovasculature have been actively pursued in anticancer drug discovery. Although many diverse stimuli are implicated in angiogenesis, signaling induced by vascular endothelial growth factor (VEGF) is considered rate limiting [1, 2], which regulates key processes throughout the angiogenic cascade, such as endothelial cell migration and proliferation, capillary tube formation and neovascular survival [3, 4]. Vascular endothelial growth factor receptors (VEGFR) are the specific transmembrane receptors for VEGF, which belong to receptor tyrosine kinase and mainly include VEGFR-1, VEGFR-2 and VEGFR-3. Activation of VEGFR, especially VEGFR-2, has been demonstrated the major stimulator of angiogenesis; in contrast, inhibition of the VEGFR function results in regression of preformed tumor vessels and could subsequently lead to extensive tumor necrosis [4, 5].

Inhibition of VEGF-VEGFR pathway, either through the receptor or the ligand, has gained clinical proof of concept of being an effective approach to anticancer therapy, as seen from the commercialized monoclonal antibody bevacizumab and small molecule tyrosine kinase inhibitors (TKI) Sunitinib [6], Sorafenib [7] and Pazopanib [8]. The landscape of TKIs targeting antiangiogenesis is expanding rapidly, with an increasing number of agents currently under the different phases of drug development [4, 5]. However, most of them, including Sunitinib, Sorafenib and Pazopanib, are inherently multi-targeted inhibitors, potently inhibiting a wide range of tyrosine kinases and other targets [5, 8]. Although the systemic network of tumorigenesis

has been recognized and multiple-target intervention in cancer therapy is increasingly advocated [9], there is still a perception that multi-targeted inhibitors are inherently toxic resulting from target non-selectivity. For Sunitinib, Sorafenib and Pazopanib, the lack of specificity for the VEGFR with the relatively low potency is manifested in the high clinical doses and the occurrence of several toxicities that are unrelated to blockage of the VEGF pathway and have not been observed with the monoclonal antibody bevacizumab, which requires dose reductions or interruptions [8, 10]. The off-target effects have also limited their use in combination regimens due to overlapping toxicities with chemotherapeutic agents. In this consequence, it is rationally necessary to develop a more selective and potent small molecule VEGFR inhibitors with desirable pharmacokinetics to improve current treatments, as exemplified by axitinib [11, 12].

Here we described Fruquintinib (HMPL-013), a highly selective and potent TKI targeting VEGFR currently under the clinical development. The present work was conducted to investigate the preclinical pharmacokinetics (PK) and absorption, distribution, metabolism and excretion (ADME) properties and to predict human pharmacokinetics and efficacious dose of HMPL-013 to support its clinical trials.

## Materials and methods

The materials of HMPL-013 were provided by Departments of Medicinal Chemistry and Department of Pharmaceutical Sciences, Hutchison MediPharma Ltd. ICR mice (20–30 g), SD rats (180–250 g), Beagle dogs (8.2–10.8 kg) and Cynomolgus monkeys (4–7 kg) were all obtained from standard vendors in China with certificates of laboratory animal production and usage. HTS Transwell® 24-well Culture Plate Inserts (Surface area: 0.33 cm<sup>2</sup>, polycarbonate membrane, pore diameter: 0.4 μm) were purchased from Corning Costar, USA. Rapid Equilibrium Dialysis (RED) device with an 8000 dalton molecular weight cutoff was purchased from Thermo Fisher Scientific Inc, USA. Liver microsomes were purchased from BD Biosciences, USA or Research Institute for Liver Diseases (Shanghai) Co. LTD. Monoclonal antibodies of cytochrome P450 (CYP) isoforms were purchased from BD Bioscience, USA. Human primary cultured hepatocytes (Lot number: DFSA) were obtained from Research Institute for Liver Diseases (Shanghai) Co. Ltd. Otherwise noted, all other materials were obtained from standard vendors and of high quality.

Pharmacokinetics in mouse, rat, dog and monkey

The in vivo PK studies were conducted under the approvals from related institutional animal care and use

committees. PK studies in mouse and monkey were conducted with an exploratory purpose at doses arbitrarily chosen, while the definite PK studies were conducted in rat and dog at the doses which were rationally selected based on scientific considerations. Otherwise noted, animals were fasted overnight until 4 h post-dose. Water was supplied ad libitum. An intravenous bolus dosing was executed within 1 h after the dosing solution was prepared. The blood sample was harvested with sodium heparin as anticoagulant. The plasma was separated by centrifugation and stored at no higher than  $-70\text{ }^{\circ}\text{C}$  until analysis. Plasma concentrations were determined using the methods described in the following “[Quantitative sample analysis](#)” section.

#### *Single-dosing mouse PK study*

Twelve male mice were randomly divided into two groups (6 mice per group). One group was given an intravenous dose of 2.5 mg/kg dissolved in saline containing 10 % Solutol<sup>®</sup> HS 15 and 10 % ethanol with pH adjusted to 3.5. The other group was given an oral dose of 10 mg/kg as a suspension in 0.5 % CMC-Na. In each group, 3 mice were blood sampled at pre-dose (0), 0.25, 1, 2, 6 and 24 h post-dose, while the remaining at 5 min, 0.5, 1.5, 4 and 8 h post-dose. At the due time, 100  $\mu\text{L}$  of blood was collected.

#### *Single-dosing rat PK study*

Twenty-four rats of both genders were randomly divided into four groups (3 male and 3 female for each group). One group was given an intravenous dose of 1 mg/kg dissolved in saline containing 10 % Solutol<sup>®</sup> HS 15 and 10 % ethanol and acidified by 0.3 mL of 0.2 M hydrochloric acid. The other three groups were orally given HMPL-013 at 0.5, 1 and 2 mg/kg, respectively, as suspended in 0.5 % CMC-Na. The blood sampling time points were pre-dose (0), 5, 15 and 30 min, 1, 2, 4, 6, 8, 12 and 24 h post-dose for intravenous dosing and pre-dose (0), 30 min, 1, 2, 3, 4, 5, 7, 9, 12 and 24 h post-dose for oral administrations. 100  $\mu\text{L}$  of blood was serially collected at due time.

#### *Single-dosing dog PK study*

Active pharmaceutical ingredient (API) and formulated capsule ingredient (with the same lot of API used) of HMPL-013 were used in dog PK study. The doses listed hereafter were all API-equivalent. 18 dogs of both genders were randomly divided into 3 groups with 3 males and 3 females each. Group 1 received an intravenous dose of 0.3 mg/kg HMPL-013 in Period 1, and an oral dose of 0.3 mg/kg (formulated ingredient) in Period 2. Group

2 received an oral dose of 0.1 mg/kg (formulated ingredient) in Period 1, and an oral dose of 0.3 mg/kg (API) in Period 2. Group 3 was given an oral dose of 1 mg/kg (formulated ingredient) in Period 1, while in Period 2, this group was fed with normal canine food 30 min just before it received the same dosing regimen as in Period 1. Periods were separated by a washout time of 7 days. The intravenous dosing solution was prepared by dissolving HMPL-013 API in saline containing 10 % Solutol<sup>®</sup> HS 15 and 10 % ethanol and acidified by 0.3 mL of 0.2 M hydrochloric acid. Oral preparations were made by loading appropriate amount of HMPL-013, either formulated ingredient or API, into TORPAC<sup>®</sup> veterinary capsules (Torpac Inc., USA), according to the animal body weight (1 dog, 1 capsule). The blood sampling time points were pre-dose (0), 5 min, 0.5, 1, 2, 3, 4, 5, 7, 9, 12, 16, 24, 30, 36 and 48 h post-dose for intravenous dosing and pre-dose (0), 0.5, 1, 2, 3, 4, 5, 7, 9, 12, 16, 24, 30, 36 and 48 h post-dose for oral administrations. At the due time, 0.5 mL of blood was serially collected.

#### *Single-dosing monkey PK study*

Three male and 3 female monkeys were used. Half the monkeys were randomly selected to receive an intravenous dose of 0.5 mg/kg with the same formulation used in mouse PK study in Period 1, and an oral dose of 1 mg/kg as a suspension in saline containing 1.5 % of 0.2 M hydrochloric acid in Period 2; the other half were given an oral dose in Period 1, while an intravenous dose in Period 2. A 10-day washout time separated each period. 0.5 mL of blood was sampled at each time point as follow: pre-dose (0), 2, 10, 30 min, 1.5, 2, 3, 4, 6, 8, 12, 16, 24, 36, 48 and 60 h for intravenous dosing and pre-dose (0), 10, 30 min, 1, 1.5, 2, 3, 4, 6, 8, 12, 16, 24, 36, 48 and 60 h for oral dosing.

#### *PK data analysis and statistical analysis*

PK data analysis was performed on the plasma concentration–time data from individual animals (rat, dog and monkey) or on mean plasma concentration–time data (mouse). PK parameters were determined based on non-compartmental analysis using Kinetica<sup>®</sup> software (Version 4.4.1, Thermo Electron Corporation, USA) for mouse PK data and DAS software (Version 2.0, China Pharmacological Society) for rat, dog and monkey PK data. Student *t* test was employed for the log-transformed area under the concentration–time curve from time zero to infinity ( $\text{AUC}_{\text{inf}}$ ) and the maximal concentration ( $C_{\text{max}}$ ) to evaluate the statistical significance of difference, while Wilcoxon signed rank test for the time to reach the maximal concentration ( $T_{\text{max}}$ ).

## Absorption

### *In vitro transport study across Caco-2 cell monolayer*

Caco-2 cell culture and monolayer preparation were performed according to reported methods [13] with modifications. Caco-2 cells were seeded at a density of  $2 \times 10^5$  cells/mL. Transport studies were conducted with the monolayers cultured for approximately 21 days, and the cell passage numbers were between 45 and 65. The transport medium buffer was modified Hank's balanced salt solution containing 10 mM HEPES and 0.1  $\mu$ M of propranolol (analytical internal standard (IS)). The pH of both the apical and basolateral compartments was 7.4. The bi-directional transport studies were initiated by adding an appropriate volume of buffer containing HMPL-013 to either the apical or basolateral side of the monolayer. Concentration-dependent transport of HMPL-013 was evaluated at 0.5, 1 and 5  $\mu$ M after 60-min incubation, while time-dependent transport of HMPL-013 was evaluated at 1  $\mu$ M after incubation for 60, 90 and 120 min. At 1  $\mu$ M with incubation for 60 min, transport of HMPL-013 was also assessed in the presence of verapamil at 10  $\mu$ M. After incubation for a due time, the samples of both sides were collected for analysis. The peak area ratios of HMPL-013 and digoxin toward IS were determined. Apparent permeability coefficient ( $P_{app}$ ) and the efflux ratio (ER) were assessed with the equations as followed:

$$P_{app} = \frac{V_r \times R_{r,t}}{S \times t \times R_{d,0}}; \text{ER} = \frac{P_{app}(B - A)}{P_{app}(A - B)}$$

where,  $R_{r,t}$ : peak area ratio in receiver at time  $t$ ;  $R_{d,0}$ : peak area ratio in donor at time zero;  $V_r$ : receiver volume;  $V_d$ : donor volume;  $S$ : surface area of the cell monolayer;  $t$ : incubation time (sec).

## Distribution

### *In vitro plasma protein binding*

The protein binding of HMPL-013 in pooled plasma of nude mouse, rat, dog and human was determined at three concentration levels (1, 3 and 10  $\mu$ M) using RED device. 200  $\mu$ L of plasma was dialyzed against 350  $\mu$ L of 20 mM phosphate buffer (pH 7.4) in a closed shaking water bath maintained at 37 °C for 6 h. Experiments were carried out in triplicates. Equilibrium at 6 h was evaluated by dialysis with HMPL-013-containing phosphate buffer. After 6 h, aliquots of buffer and plasma were taken for analysis. The spiked plasma samples at time zero were also analyzed, and the recovery was determined at the end of the dialysis to evaluate the potential

non-specific binding and compound stability. Plasma protein binding fraction (PB %) was calculated by the equation:  $\text{PB \%} = (C_p - C_b)/C_p \times 100 \%$ , where  $C_p$  was the concentration of plasma samples and  $C_b$  was the concentration of buffer samples.

### *Tissue distribution in rats*

The test compound and formulation in this study were same as those in rat PK study. 18 rats were averagely divided into three groups with 3 male and 3 female each. They all received 1 mg/kg HMPL-013 orally. The rats in the three groups were killed in turn at 2, 5 and 14 h post-dose. Tissues (brain, heart, liver, spleen, lung, kidney, bladder, pancreas, marrow, fat, ovary, uterus, testis, stomach, intestine and adrenal) were harvested, weighed and then stored at  $-20$  °C until analysis. Tissue concentrations were determined using the methods described in the following "Quantitative sample analysis" section.

## Metabolism

### *In vitro metabolic stability in liver microsomes*

The *in vitro* metabolism of HMPL-013 was investigated in liver microsomes of different species. A typical microsomal incubation mixture contained 1  $\mu$ M HMPL-013, 0.5 mg/mL liver microsomes, 3 mM magnesium chloride, 1 mM EDTA and an NADPH-regenerating system which consisted of 1 mM NADP, 5 mM glucose-6-phosphate and 1 Unit/mL glucose-6-phosphate dehydrogenase, in 50 mM potassium phosphate buffer. Incubations were performed in duplicates at 37 °C. The enzyme reaction was initiated by adding the NADPH-regenerating system and quenched at various times (0, 5, 15, 30, 60 or 120 min) by adding an equal volume (125  $\mu$ L) of ice-cold stop solution (0.5  $\mu$ g/mL phenacetin as IS in acetonitrile containing 1 % formic acid). Supernatants were subjected to liquid chromatography tandem mass spectrometry (LC/MS/MS) for analysis. The incubation of HMPL-013 with liver microsomes was also conducted after the deactivation of flavin monooxygenase (FMO) by heating for 5 min at 45 °C, with the other conditions unchanged. Apparent half-lives ( $t_{1/2}$ ) for the disappearance of HMPL-013 were calculated from the pseudo-first-order rate constants obtained by linear regression of log HMPL-013 nominal concentration (peak area ratio) vs. time plots. Intrinsic clearance and scaled hepatic clearance were further estimated according to literature methods [14–16] without correction for potential protein binding and based on the following assumptions: (1) a well-stirred model; (2) oxidative metabolism was the major mechanism of hepatic clearance.

### Exploratory *in vitro* and *in vivo* metabolite identification

The *in vitro* metabolite profiles of HMPL-013 were exploringly determined in liver microsomes of different species. Qualitative *in vivo* metabolite identification (MID) was performed using rat plasma, bile, urine and feces.

For *in vitro* MID, the test compound and the incubation mixture were same as those mentioned in the “[In vitro metabolic stability](#)” section, except HMPL-013 concentration was 50  $\mu\text{M}$ . Incubations were performed at 37 °C for 30 min or 2 h. Reactions were quenched by the addition of an equal volume of acetonitrile and centrifugation followed. Supernatants (injection volume 20  $\mu\text{L}$ ) were subjected to LC/MS/MS analysis, which was performed using an API4000QTrap mass spectrometer (Applied Biosystems, USA), coupled through a TurboIonSpray interface with an Agilent 1200 LC system equipped with a diode array detector. LC column was a Zorbax SB-C18 column (4.6  $\times$  150 mm; 5  $\mu\text{m}$ ) (Agilent, USA). Mobile phases consisted of phase A with 0.1 % formic acid in water and phase B with 0.1 % formic acid in acetonitrile. Gradient elution with flow rate of 1 mL/min lasted for 30 min. The ultraviolet (UV) absorbance wavelength was set at 254 nm. Metabolites were identified based upon their protonized molecular ions and fragmentation patterns, by iteratively using enhance Q1 full scan and enhanced product ion scan, with the aid of UV chromatograms.

For *in vivo* MID, rat plasma was from rat PK studies; rat bile, urine and feces were obtained as described in the following “[Excretion](#)” section 400  $\mu\text{L}$  of methanol was added to 200  $\mu\text{L}$  of bile or urine. 200  $\mu\text{L}$  of methanol was added to 50  $\mu\text{L}$  of plasma. Fecal samples were grinded and 0.2 g of aliquot was weighed, followed by addition of 1 mL methanol. After extraction and centrifugation, the supernatant was evaporated and the residue was reconstituted in 150  $\mu\text{L}$  of a mixed solution containing acetonitrile and 5 mM ammonium acetate aqueous solution (10:90, v/v). 10  $\mu\text{L}$  of the reconstituted solution was subjected to LC/MS/MS analysis, which was performed using a Synapt Q-TOF mass spectrometer (Waters, USA), coupled through an electrospray interface with an UPLC system (Waters, USA). LC column was an Acquity UPLC™ BEH C-18 column (2.1  $\times$  100 mm; 1.7  $\mu\text{m}$ ) (Waters, USA). Mobile phases consisted of phase A with 5 mM ammonium acetate in water and phase B with 0.05 % formic acid in acetonitrile. Gradient elution with flow rate of 0.4 mL/min lasted for 21 min. Metabolites were identified based upon their protonized molecular ions and fragmentation patterns.

### CYP reaction phenotyping

After three major *in vitro* metabolites were identified (see “[Result](#)” section), the contribution of CYP enzymes to

each metabolite formation was estimated in human liver microsomes using monoclonal antibodies. Antibodies with appropriate volume were firstly added to ice-bathed microsomes for a pre-incubation of 20 min. Then potassium phosphate buffer containing HMPL-013 was added, followed by the addition of pre-warmed NADPH-regenerating system to initiate the reaction. Except for the antibodies, the final incubation system was same as those used for *in vitro* MID. After 30 min, the incubation was quenched by adding an equal volume of ice-cold stop solution (0.5  $\mu\text{g}/\text{mL}$  phenacetin as IS in acetonitrile containing 1 % formic acid). Supernatants were subjected to LC/MS/MS to determine the relative amount of a formed metabolite. The antibody activities toward 1A2, 2C8, 2C19, 2D6 and 3A4 were positively controlled by the appropriate probe substrates/metabolites (see the following “[CYP inhibition](#)” section). The percentage of the relative amount of a given metabolite after antibody treatment to that without antibody treatment (negative control) was calculated to reflect a CYP isoform contribution to the formation of this given metabolite.

### CYP inhibition

Reversible CYP inhibition by HMPL-013 was evaluated over a concentration range of 0.08–50  $\mu\text{M}$  using human liver microsomes. A typical incubation mixture contained HMPL-013, probe substrate, 0.2 mg/mL liver microsomes (except 0.5 mg/mL for 2C19), 3 mM magnesium chloride, 1 mM EDTA and an NADPH-regenerating system with the same constituents described before. Incubations were performed in duplicates at 37 °C. The enzyme reaction was initiated by adding the NADPH-regenerating system and quenched at 20 min (except 30 min for 2C19 and 10 min for 3A4-midazolam reaction) by adding an equal volume of ice-cold acetonitrile containing different IS (diazepam for 1A2, 7-hydroxycoumarin for 2C9, hydrocortisone for 2C19 and cortisone for 2C8, 2D6 and 3A4). The supernatants were separated for analysis. Reaction conditions were previously determined to result in a linear rate of formation of CYP-specific metabolites. The activity of each CYP isoform was determined using the following probe substrates/metabolites (substrate concentrations showed in parentheses): phenacetin (50  $\mu\text{M}$ )/acetaminophen for 1A2, paclitaxel (10  $\mu\text{M}$ )/6 $\alpha$ -hydroxypaclitaxel for 2C8, diclofenac (5  $\mu\text{M}$ )/4'-hydroxydiclofenac for 2C9, *S*-mephenytoin (20  $\mu\text{M}$ )/4'-hydroxymephenytoin for 2C19, dextromethorphan (6  $\mu\text{M}$ )/dextrorphan for 2D6, testosterone (45  $\mu\text{M}$ )/6 $\beta$ -hydroxytestosterone for 3A4, and midazolam (5  $\mu\text{M}$ )/1'-hydroxymidazolam also for 3A4. The formation of probe metabolites was analyzed by LC/MS/MS. Parallely,  $\alpha$ -naphthoflavone, quercetin, sulfaphenazole, ticlopidine, quinidine and ketoconazole at suitable concentrations were used as positive inhibitors of 1A2, 2C8, 2C9, 2C19,



2D6 and 3A4, respectively. The remaining activities of each CYP isoform were fitted to the various concentrations of inhibitors using nonlinear least-squares regression to determine the inhibition  $IC_{50}$ .

Time-dependent CYP inhibition of HMPL-013 was evaluated at 10  $\mu$ M in human liver microsomes with an exploratory purpose. HMPL-013 was mixed with human liver microsomes (final concentration: 0.5 mg/mL) and pre-incubated in absence and presence of NADPH-regenerating system. After pre-incubated for 30 min at 37 °C, this incubation mixture was diluted one-fourth fold with buffer containing probe substrate of each CYP isoform. Another appropriate volume of NADPH-regenerating system was added to initiate the second step of reaction. After incubated for another 30 min at 37 °C, the ice-cold acetonitrile containing IS was added to quench the reaction. Regarding to the second step of reaction, the activity of each CYP isoform was determined using the same probe substrates/metabolites as mentioned in the previous paragraph. The activity of each CYP isoform in presence of NADPH in the first incubation was compared with that in absence of NADPH in the first incubation to roughly estimate the extent of time-dependent inhibition. Furafylline (1  $\mu$ M) and azamulin (0.5  $\mu$ M) were used as positive time-dependent inhibitors to CYP1A2 and CYP3A4, respectively.

#### CYP induction

The CYP3A4 induction potential caused by HMPL-013 was firstly analyzed by evaluation of the human pregnane X receptor (hPXR)-mediated transactivation of CYP3A4 in HepG2 cell-based luciferase reporter gene assay. In brief, HepG2 cells were co-transfected with hPXR-expressing (pcDNA4-hPXR) plasmid and the plasmid expressing CYP3A4-luciferase reporter gene via liposomes. The cells were then treated with RPMI-1640 culture media containing 10  $\mu$ M of HMPL-013 and 10  $\mu$ M of two positive control inducers (rifampicin and ritonavir), respectively. Parallely, the transfected cells were also treated with RPMI-1640 culture media containing 0.3 % DMSO as the vehicle baseline control. Each treatment had five replicates. After 24 h, the luciferase activity was determined by the Steady-Glo Luciferase Assay Kit (Promega, USA). The induction fold was obtained by dividing the luciferase activities of inducer-treated wells to those of the baseline control wells. The induction potential of HMPL-013 was evaluated by comparing its induction fold with those of the positive controls.

Secondly, the CYP induction potential of HMPL-013 was investigated in human primary cultured hepatocytes. In parallel, the hepatocytes were incubated with HMPL-013 at 10  $\mu$ M, positive CYP1A2 inducer omeprazole at 100  $\mu$ M, positive CYP3A4 inducer rifampin at 50  $\mu$ M, and blank culture media containing vehicles as the negative control,

respectively. After incubation for 3 days, the culture media were replaced and the hepatocytes were further incubated with probe substrates of CYP1A2 (phenacetin 50  $\mu$ M) and CYP3A4 (testosterone 100  $\mu$ M) for 60 min, respectively. Then, an equal volume of pre-cold methanol was added to the incubate. After centrifugation, supernatants were collected for LC/MS/MS analysis. The formation of acetaminophen and 6 $\beta$ -hydroxytestosterone was determined to evaluate the 1A2 and 3A4 activities, respectively. All incubations were conducted at 37 °C with 5 %  $CO_2$ . The sample size was at least triplicates. The inducible potential was reported by using relative activity of CYP isoforms as percentage to negative control (induction fold).

#### Excretion

The test compound and formulation in this study were the same as those in rat PK study. Samples of plasma, bile, urine and feces were kept at  $-20$  °C until analysis. The concentrations of HMPL-013 and two metabolites in rat excreta were determined using the methods described in the following “Quantitative sample analysis” section.

#### Rat urinary and fecal excretion

Six rats of both genders were administered orally with 1 mg/kg HMPL-013 and subsequently housed in individual metabolic cages. Urine and feces were separately gathered during the intervals of  $-24$  to 0 h pre-dose and 0–6, 6–12, 12–24, 24–36 and 36–48 h post-dose. The volume of urine and the weight of feces in each interval were measured.

#### Rat biliary excretion

Six rats of both genders surgically received bile duct cannula insertion after anesthesia. After recovered from surgery, the rats were orally administered at 1 mg/kg HMPL-013, and bile samples were collected from 0–6, 6–12 and 12–24 h. The volume of bile in each interval was measured.

#### Excretion data analysis

Renal clearance ( $CL_R$ ) and biliary clearance ( $CL_B$ ) of the unchanged HMPL-013 was calculated using the following equations:

$$CL_R = \frac{A_{\text{excreted,U,P}}}{AUC_{\text{inf}}}, CL_B = \frac{A_{\text{excreted,B,P}}}{AUC_{\text{inf}}}$$

$A_{\text{excreted,U,P}}$ : total excreted amount of parent drug in urine;  
 $A_{\text{excreted,B,P}}$ : total excreted amount of parent drug in bile;  
 $AUC_{\text{inf}}$ : the corresponding overall average plasma  $AUC_{\text{inf}}$  in rat PK study after oral administration at 1 mg/kg (1,134 ng/mL  $\times$  h, see Table 1).

The cumulative excretion rate (CER) of each analyte (HMPL-013 and the two metabolites) was calculated separately using the following equation:

$$\text{CER} = \frac{\sum A_{\text{excreted}}}{A_{\text{dosed}}} \times 100\%$$

$A_{\text{excreted}}$ : excreted amount of each analyte;  $A_{\text{dosed}}$ : dosed amount. Mass balance recovery was roughly estimated by summarizing the CER of each analyte in urine and feces.

#### Quantitative sample analysis

##### *Quantitative analysis in mouse and monkey PK study*

With the exploratory purpose, the plasma samples in mouse and monkey PK studies were analyzed using non-validated methods. 50  $\mu\text{L}$  aliquot of plasma samples were protein-precipitated by adding two or three fold volume of acetonitrile containing appropriate amount of IS phenacetin. The supernatant was either diluted with equal volume of water before injection (mouse) or directly (monkey) subject to LC/MS/MS analysis (injection volume 10  $\mu\text{L}$ ). The machines were an API4000 mass spectrometer (Applied Biosystems, USA) coupled with an Agilent 1200 HPLC system and a HTC PAL autosampler (CTC Analytics AG, Switzerland) for mouse study, and an API3000 mass spectrometer (Applied Biosystems, USA) coupled with LC-10AD pumps (Shimadzu, Japan) and MPS3C autosampler (Gerstel, Germany) for monkey study. The interfaces were both TurboIonSpray. Chromatography was achieved using a Symmetry C18 column (2.1  $\times$  50 mm; 3  $\mu\text{m}$ , Waters, USA) for mouse study and a CAPCELL PAK C18 column (2.0  $\times$  30 mm; 3  $\mu\text{m}$ , Shiseido, Japan) for monkey study. Mobile phases were same; both consisted of phase A with 0.1 % formic acid in water and phase B with 0.1 % formic acid in acetonitrile. A 3.5-min fast gradient elution was performed, with the flow rate of either 1 (mouse) or 0.25 (monkey) mL/min. The positive-ion multiple reaction monitoring (MRM) transition of  $m/z$  394 to 363 was used for detection of HMPL-013 with the optimal ion source and MS parameters. The lower limit of quantification (LLOQ) of HMPL-013 was 2.4 ng/mL in mouse study, and the quantification range of HMPL-013 was 0.5–2,000 ng/mL in monkey study.

##### *Quantitative analysis in rat and dog studies*

This method underwent full validation in rat and dog plasma and partial validation in rat tissues, bile, urine and feces samples, according to the FDA guidance [17]. The IS was a HMPL-proprietary structural analog. Only parent HMPL-013 was determined in PK and tissue distribution studies. In rat excretion studies, HMPL-013 and two phase I metabolites HM5013199 (M1) and HM5012569 (M2)

identified in vitro were simultaneously determined with and without the glucuronidase enzymolysis.

For plasma samples, 25  $\mu\text{L}$  of IS solution (100 ng/mL in methanol), 25  $\mu\text{L}$  of methanol and 100  $\mu\text{L}$  of acetonitrile was sequentially added to 25  $\mu\text{L}$  aliquot of plasma samples, followed by vortexing and centrifugation. The supernatants were evaporated and the residue was reconstituted in 150  $\mu\text{L}$  of mobile phase, which was a mixture of acetonitrile and 10 mM ammonium acetate aqueous solution containing 0.1 % formic acid (45:55, v/v). 20  $\mu\text{L}$  of the reconstituted solution was subjected to LC/MS/MS analysis.

Rat tissues were firstly weighed to aliquot and fivefold volume of methanol was added. Tissue homogenates were obtained after homogenization, sonication and centrifugation. The following pretreatment procedures were same as those for plasma samples.

Regarding to direct analysis of excreta samples without enzymolysis, 25  $\mu\text{L}$  of IS solution (100 ng/mL in methanol), 25  $\mu\text{L}$  of methanol and 500  $\mu\text{L}$  of mobile phase was sequentially added to 25  $\mu\text{L}$  aliquot of urine or bile samples, followed by vortexing and centrifugation. 20  $\mu\text{L}$  of the supernatants were subjected to LC/MS/MS analysis. Feces were firstly weighed to 200 mg aliquot and 1 mL of methanol was added. Following vortexing and repeated sonication, the fecal samples were centrifuged and the supernatant was obtained as feces homogenates. 25  $\mu\text{L}$  of the feces homogenates was mixed with 25  $\mu\text{L}$  of IS solution and 150  $\mu\text{L}$  of mobile phase sequentially, followed by vortexing and centrifugation as well. 20  $\mu\text{L}$  of the supernatants were subjected to LC/MS/MS analysis.

Regarding to analysis of excreta samples after glucuronidase enzymolysis, 50  $\mu\text{L}$  of urine or bile sample aliquot was mixed with 200  $\mu\text{L}$  of  $\beta$ -glucuronidase (2,000 unit/mL) and incubated for 16 h at 37  $^{\circ}\text{C}$ . After incubation, 100  $\mu\text{L}$  of IS-containing acetonitrile was added to 25  $\mu\text{L}$  aliquot of the incubated sample. Following vortexing and centrifugation, the supernatants were evaporated and the residue was reconstituted in 100  $\mu\text{L}$  of mobile phase. 20  $\mu\text{L}$  was subjected to LC/MS/MS analysis. 50  $\mu\text{L}$  of feces homogenates was firstly dried under 40  $^{\circ}\text{C}$ , followed by the addition of 200  $\mu\text{L}$  of  $\beta$ -glucuronidase (2,000 unit/mL) and incubation for 16 h at 37  $^{\circ}\text{C}$ . After incubation, 100  $\mu\text{L}$  of IS-containing acetonitrile was added to 100  $\mu\text{L}$  of the incubated sample.

Twenty  $\mu\text{L}$  of the supernatant was analyzed with LC/MS/MS on an API4000 mass spectrometer (Applied Biosystems, USA) coupled through an atmospheric pressure chemical ionization (APCI) interface with LC-20AD pumps and SIL-HTA autosampler (Shimadzu, Japan). Chromatography was achieved using a Zorbax C18 column (4.6  $\times$  150 mm; 5  $\mu\text{m}$ , Agilent, USA). Isocratic elution was carried out with flow rate at 0.7 mL/min. The positive-ion MRM transition of  $m/z$  394 to 363 was used for detection of HMPL-013 with the optimal ion source

**Table 1** Pharmacokinetic parameters (mean  $\pm$  SD, if applicable) of HMPL-013 in mouse, rat, monkey and dog following single IV and PO administrations

IV administration		PO administration															
Dose (mg/kg)	Sex <sup>a</sup>	No. of animals	CL (mL/min/kg)	V <sub>z</sub> (L/kg)	t <sub>1/2</sub> (h)	MRT <sub>inf</sub> (h)	AUC <sub>inf</sub> (ng/mL $\times$ h)	Dose <sup>d</sup> (mg/kg)	Sex <sup>a</sup>	No. of animals	AUC <sub>inf</sub> (ng/mL $\times$ h)	C <sub>max</sub> (ng/mL)	T <sub>max</sub> (h)	t <sub>1/2</sub> (h)	MRT <sub>inf</sub> (h)	F (%) <sup>b</sup>	
Mouse	2.5	M	6 (3/point)	3.3	0.7	2.4	3.4	10,497	10	M	6 (3/point)	17,649	2,057	2.0	2.0	5.4	43.2
Rat									0.5	M	3	248 $\pm$ 99.0	86.7 $\pm$ 23.1	1.7 $\pm$ 0.6	0.9 $\pm$ 0.4	2.3 $\pm$ 0.6	
										F	3	365 $\pm$ 191	82.1 $\pm$ 27.7	2.0 $\pm$ 0.0	1.4 $\pm$ 0.4	3.5 $\pm$ 0.9	
										O	6	307 $\pm$ 150	84.4 $\pm$ 23.0	1.8 $\pm$ 0.4	1.2 $\pm$ 0.4	2.9 $\pm$ 0.9	
	1	M	3	10.0 $\pm$ 3.4	0.7 $\pm$ 0.1	0.9 $\pm$ 0.2	1.2 $\pm$ 0.3	1,775 $\pm$ 509.0	1	M	3	870 $\pm$ 362	279 $\pm$ 121	1.7 $\pm$ 0.6	1.4 $\pm$ 0.5	2.7 $\pm$ 0.4	49.0
		F	3	6.0 $\pm$ 2.3	0.6 $\pm$ 0.1	1.2 $\pm$ 0.3	1.7 $\pm$ 0.5	3,087 $\pm$ 1,198		F	3	1,398 $\pm$ 22.0	374 $\pm$ 11.0	2.0 $\pm$ 0.0	1.3 $\pm$ 0.2	3.3 $\pm$ 0.1	45.3
		O	6	8.0 $\pm$ 3.4	0.7 $\pm$ 0.1	1.0 $\pm$ 0.3	1.4 $\pm$ 0.5	2,431 $\pm$ 1,093	2	O	6	1,134 $\pm$ 369	326 $\pm$ 93.0	1.8 $\pm$ 0.4	1.4 $\pm$ 0.3	3.0 $\pm$ 0.4	46.6
Monkey	0.5	M	3	8.7 $\pm$ 0.3	4.2 $\pm$ 1.6	5.6 $\pm$ 2.4	2.5 $\pm$ 0.3	953.5 $\pm$ 41.85	1	M	3	657.5 $\pm$ 249.7	126 $\pm$ 19.3	2.0 $\pm$ 1.0	3.9 $\pm$ 0.5	8.8 $\pm$ 1.9	34.7 $\pm$ 13.9
		F	3	6.9 $\pm$ 7.9	2.6 $\pm$ 3.1	4.4 $\pm$ 0.4	4.6 $\pm$ 2.6	2,872 $\pm$ 2,371		F	3	2,548 $\pm$ 1,868	233 $\pm$ 143	4.3 $\pm$ 3.2	4.1 $\pm$ 0.7	6.2 $\pm$ 0.4	47.1 $\pm$ 6.3
		O	6	7.8 $\pm$ 5.1	3.4 $\pm$ 2.3	5.0 $\pm$ 1.7	3.6 $\pm$ 2.1	1,913 $\pm$ 1,831		O	6	1,603 $\pm$ 1,579	179 $\pm$ 108	3.2 $\pm$ 2.5	4.0 $\pm$ 0.6	7.5 $\pm$ 1.9	41.9 $\pm$ 11.8
Dog									0.3API	M	3	1,877 $\pm$ 535	123 $\pm$ 44	3.0 $\pm$ 1.0	9.1 $\pm$ 2.5	17.6 $\pm$ 0.7	54.4
										F	3	1,535 $\pm$ 619	78.3 $\pm$ 42.4	2.7 $\pm$ 1.2	12.3 $\pm$ 1.3	19.9 $\pm$ 0.4	37.8
										O	6	1,706 $\pm$ 551	101 $\pm$ 46	2.8 $\pm$ 1.0	10.7 $\pm$ 2.5	18.8 $\pm$ 1.4	45.4
Dog									0.1 formulation	M	3	759 $\pm$ 235	57.2 $\pm$ 20.9	2.3 $\pm$ 0.6	12.2 $\pm$ 1.8	17.0 $\pm$ 1.2	
										F	3	822 $\pm$ 210	62.9 $\pm$ 16.2	3.0 $\pm$ 1.0	10.8 $\pm$ 3.6	16.9 $\pm$ 3.8	
										O	6	791 $\pm$ 202	60.1 $\pm$ 17.0	2.7 $\pm$ 0.8	11.52.7	17.0 $\pm$ 2.5	
	0.3	M	3	1.5 $\pm$ 0.1	1.7 $\pm$ 0.6	13.4 $\pm$ 4.0	18.3 $\pm$ 2.4	3,453 $\pm$ 326	0.3 formulation	M	3	2,338 $\pm$ 487	160 $\pm$ 48	4.0 $\pm$ 0.0	15.9 $\pm$ 1.1	22.7 $\pm$ 1.7	68.5 $\pm$ 17.4
		F	3	1.2 $\pm$ 0.1	1.6 $\pm$ 0.1	14.6 $\pm$ 0.5	19.5 $\pm$ 0.9	4,057 $\pm$ 167		F	3	1,756 $\pm$ 970	98.6 $\pm$ 57.0	4.0 $\pm$ 0.0	15.4 $\pm$ 0.9	22.7 $\pm$ 0.9	43.5 $\pm$ 24.8
		O	6	1.3 $\pm$ 0.1	1.6 $\pm$ 0.4	14.0 $\pm$ 2.6	18.9 $\pm$ 1.7	3,755 $\pm$ 404	1 formulation	O	6	2,047 $\pm$ 757	129 $\pm$ 58	4.0 $\pm$ 0.0	15.7 $\pm$ 0.9	22.7 $\pm$ 1.2	56.0 $\pm$ 23.6
										M	3	6,140 $\pm$ 3,522	359 $\pm$ 243	3.7 $\pm$ 0.6	14.0 $\pm$ 6.8	23.0 $\pm$ 6.1	
										F	3	5,997 $\pm$ 655	345 $\pm$ 38	4.0 $\pm$ 0.0	14.4 $\pm$ 5.2	23.1 $\pm$ 3.5	
										O	6	6,068 $\pm$ 2,267	352 $\pm$ 156	3.8 $\pm$ 0.4	14.2 $\pm$ 5.4	23.0 $\pm$ 4.4	
									1 formulation fed <sup>d</sup>	M	3	10,132 $\pm$ 2,546	316 $\pm$ 57	3.0 $\pm$ 0.0	19.1 $\pm$ 11.4	30.5 $\pm$ 10.2	
										F	3	8,455 $\pm$ 2,395	274 $\pm$ 85	4.3 $\pm$ 2.5	12.4 $\pm$ 4.3	23.1 $\pm$ 2.2	
										O	6	9,293 $\pm$ 2,394	295 $\pm$ 69	3.7 $\pm$ 1.8	15.8 $\pm$ 8.5	26.8 $\pm$ 7.7	

<sup>a</sup> Sex item, *M* male; *F* Female; *O* Overall, male plus female<sup>b</sup> Absolute bioavailability, based on IV exposures. If self-control was applicable, F was calculated based on individual animal data. Otherwise, F was calculated based on the mean AUC<sub>inf</sub> data<sup>c</sup> This group was fed with normal canine food 30 min just before dosing. All other PO dosing, including for mouse, rat and monkey, were performed under fasted condition<sup>d</sup> In mouse, rat and monkey PK studies, the materials for oral dosing were all active pharmaceutical ingredient (API). Doses used for oral dosing in dog PK were all API-equivalent doses



and MS parameters. LLOQ of HMPL-013 in rat and dog plasma was 0.5 ng/mL, and the upper limit of quantification was 2,000 ng/mL. The quantification range of HMPL-013 in rat tissues was 2.5–10,000 ng/g. For HMPL-013, HM5012569 and HM5013199, the quantification ranges were all 5–5,000 ng/mL in urine and bile and 5–5,000 ng/g in feces. Method validation supported up to 50-fold dilution for plasma and 25-fold dilution for bile, urine and tissue/feces homogenates.

#### Quantitative analysis in *in vitro* assays

All the *in vitro* samples to be quantitated were diluted with appropriate matrices at different extent, followed by direct LC/MS/MS injection or protein-precipitated by acetonitrile before LC/MS/MS injections. Instrument analysis of HMPL-013 was based on the instruments and conditions same as those for mouse PK study, except the CYP reaction phenotyping study which has been described before. In transport and metabolic stability assays, peak area ratios were recorded, while concomitant calibration curves in plasma protein binding assay were constructed to determine the real concentrations. Specifically, in the CYP reaction phenotyping study, the relative amount of the HMPL-013 metabolites was semi-quantitatively measured by recording the peak area ratios of the metabolite to the IS. Positive compounds and CYP probe metabolites were quantitated based on their specific MRM transitions according to related institutional SOP methods.

#### Human PK prediction

The human primary PK parameters, plasma total clearance (CL) and volume of distribution at the terminal phase ( $V_z$ ), were predicted using allometric method. Firstly, the animal CL and  $V_z$  was transferred to  $CL_u$  (free drug clearance) and  $V_{z,u}$  (free drug volume) by the correction of free drug fraction in plasma ( $f_u$ ) of the corresponding species (an average value derived from data in Table 4) [18]. As monkey  $f_u$  was not available, the PK parameters obtained in cynomolgus monkey was excluded for the allometry. The  $f_u$  in ICR mouse was assumed to be identical to the  $f_u$  in nude mouse. Secondly, the  $CL_u$  in mouse, rat and dog was scaled to  $CL_u$  in human based on the body weight (BW) following the rule of exponents (RoE) [19]. The  $V_{z,u}$  in mouse, rat and dog was scaled to  $V_{z,u}$  in human simply based on BW. Finally, the  $CL_u$  and  $V_{z,u}$  in human was back converted to the CL and  $V_z$  using the  $f_u$  in human.

Human absorption-related parameters were assumed to be equivalent to those in dog based on the considerations: (1) dog was generally regarded as the preclinical PK species most similar to human regarding to the oral absorption behaviors, widely being used as the *in vivo* model to predict

human absorption; (2) in HMPL-013 dog PK study, the formulated ingredient intended for clinical usage was capped in capsules for dosing, which was similar to the human situation, in contrast, liquid formulation was used in the PK studies in other species. So, all the individual time-concentration (C-T) data from dogs orally receiving formulated ingredient under fasted condition at three dose levels (0.1, 3 and 1 mg/kg) were simultaneously modeled using a population method with Phoenix NLME (Ver 1.2, Pharsight) to get the dog absorption-related parameters. The best PK model was chose based on the minimal OFV and AIC values, together with the visual inspection of the fitness.

Human PK profile after oral administration was simulated by establishing a one-compartment oral PK model with human CL,  $V_z$  and absorption-related parameters fixed using Phoenix WinNonlin (Ver 6.3, Pharsight). The dose was set at 1 mg, which was the planned first-in-human (FIH) dose. After getting the simulated human C-T data, predicted human PK parameters, such as elimination rate constant at the terminal phase ( $\lambda_z$ ), terminal phase half life ( $t_{1/2}$ ),  $T_{max}$ ,  $C_{max}$ , CL/F (apparent CL after oral dosing),  $V_z/F$  (apparent  $V_z$  after oral dosing), mean residual time (MRT) and AUCs were obtained using the same software. Both the simulated C-T data and the predicted PK parameters were compared with the observed FIH data (internal data on file), to evaluate the goodness of prediction.

Human minimal efficacious oral dose was further predicted using the equation: Dose = CL × AUC/F, where F was the human bioavailability. Human CL was obtained from allometry as mentioned before. Human F was assumed to be as the average value (46.9 %) of the F in the four tested preclinical species, considering that cross-species variation of F was minimal (Table 1). The human AUC achieving the minimal efficacy was obtained by the following steps. Firstly, the AUC with the tumor growth inhibition (TGI) around 62 %, which was considered as the minimal efficacy in the most sensitive preclinical pharmacologic model (nude mice bearing BGC-823 xenograft), was obtained as 898 ng/mL × h (internal data on file). Secondly, this AUC in nude mice was converted to the free drug AUC ( $AUC_u$ ) by the correction of  $f_u$ . Finally, assuming the  $AUC_u$  was same in nude mice and human to achieve the same efficacy, human AUC achieving the minimal efficacy was further calculated by applying  $f_u$  in human to the assumed human  $AUC_u$ .

## Results

Pharmacokinetics of HMPL-013 in mouse, rat, dog and monkey

The semi-log plots of HMPL-013 plasma concentration versus time for mouse, rat, dog and monkey after IV and

PO administrations are presented in Fig. 1 and the derived PK parameters are listed in Table 1. Although both males and females were used in rat, dog and monkey PK studies, the statistical analysis of gender difference was not applicable due to the small sample size of each gender. But the trend clearly indicates there is no significant gender difference in rat, dog and monkey PK, if considering the individual variation. The CL of HMPL-013 in mouse, rat, dog and monkey account for 3.7, 14.5, 4.2 and 17.9 % of the hepatic blood flow of the corresponding species [20]. All of them are below the criterion of 30 % of the hepatic blood flow as low hepatic-extracted [21]. Based on the reported cardiac output [20], the body extraction ratios [22] of HMPL-013 are 0.8, 2.7, 1.1 and 3.6 % in mouse, rat, dog and monkey, respectively. All of them are below the criterion of 5 % as low body-extracted [22]. The  $V_z$  of HMPL-013 in rodent species evaluated is very close to their total body water volume (mouse: 0.725 L/kg; rat: 0.668 L/kg) [20]. But the  $V_z$  in dog and monkey is around 2.7 and 4.9-fold higher than the corresponding total body water volume (dog: 0.604 L/kg; monkey: 0.693 L/kg) [20]. The terminal half life ( $t_{1/2}$ ) is generally consistent between IV and PO dosing in all tested species, suggesting the real terminal phase was obtained and therefore confirming the accuracy of  $V_z$  and  $AUC_{inf}$  calculation in reverse. The  $t_{1/2}$  ranges from 1 to 2 h in rodent, 4–5 h in monkey and 10–15 h in dog. The species-different  $t_{1/2}$  profiles are well correlated with the extents of CL and  $V_z$  in each species. After oral administrations, HMPL-013 could achieve satisfactory exposures even in low doses. The  $T_{max}$  ranges from around 2–4 h in all tested species. The average absolute bioavailability of HMPL-013 API in mouse, rat, monkey and dog is 43.2, 46.6, 41.9 and 45.4 %, indicating a moderate oral bioavailability. Dose escalation was studied in rat and dog. Within the tested dose ranges (0.5–2 mg/kg in rat, 0.1–1 mg/kg in dog), HMPL-013 demonstrates linear PK properties.

The PK profiles of API and formulation was compared parallelly in dogs. As showed in the Plot Dog-B in Fig. 1 and Table 2, both visual inspection and statistical analysis suggested there was no significant difference between API and the tested formulation in terms of PK properties. Food effect was also assessed in dogs. As showed in the Plot Dog-C in Fig. 1 and Table 2, although statistical analysis suggested there was no significant difference between fasted and fed conditions in terms of PK properties, administration after feeding tends to slightly increase the oral absorption extent.

## Absorption

### *In vitro transport study across Caco-2 cell monolayer*

The bi-directional transport permeability and the efflux ratio of HMPL-013 across Caco-2 cell monolayers are

delineated in Table 3. HMPL-013 has high intrinsic membrane permeability with  $P_{app}$  around  $30 \times 10^{-6}$  cm/s. The transport is linear within the substrate concentrations from 0.5 to 5  $\mu$ M and time range from 1 to 2 h, as the  $P_{app}$  almost remains constant. There was no efflux transport observed in this cell line for HMPL-013, since ER were all around 1 and verapamil showed no effect on its transport.

## Distribution

### *In vitro plasma protein binding*

Dialysis equilibrium could be achieved after 6 h incubation and the recovery results, which are around 90–110 %, suggest the non-specific binding is negligible and no compound instability issue in this study (data not shown). HMPL-013 appears moderate to high plasma protein binding with  $f_u$  ranged from about 4 % in rat plasma to 12 % in dog plasma (Table 4). The  $f_u$  in human plasma is closest to rat, which is around 5 %. Protein binding is independent of concentration in the species and range of concentrations tested.

### *Tissue distribution in rats*

Tissue distribution profiles of HMPL-013 in rats were investigated by determining the concentrations in major organs after 2, 5, and 14 h post-oral-dosing at 1 mg/kg. As suggested by Fig. 2, the distribution of HMPL-013 was rapid as maximal concentration was reached at 2 h post-dosing in all examined tissues, and there was no special tissue accumulation comparing with the plasma exposures since all the tissue concentrations dropped below 50 ng/g at 14 h and were all less than 3 % of the maximal concentrations. Generally, the gastrointestinal (GI) tract and liver exhibit the highest exposures. The distributions in adipose, adrenal and kidney are slightly higher than or almost equivalent to the corresponding plasma levels. The distributions in other tissues tested are all lower than the corresponding plasma levels. The lowest distribution was observed in brain, testis and bone marrow.

## Metabolism

### *In vitro metabolic stability in liver microsomes*

As listed in Table 5, from the in vitro metabolic stability in liver microsomes of different species, the predicted hepatic clearance ( $CL_{hep,pred}$ ) was scaled from in vitro intrinsic clearance ( $CL_{int}$ ) using a well-stirred model with no correction for potential protein binding and an assumption that oxidative metabolism was the major mechanism

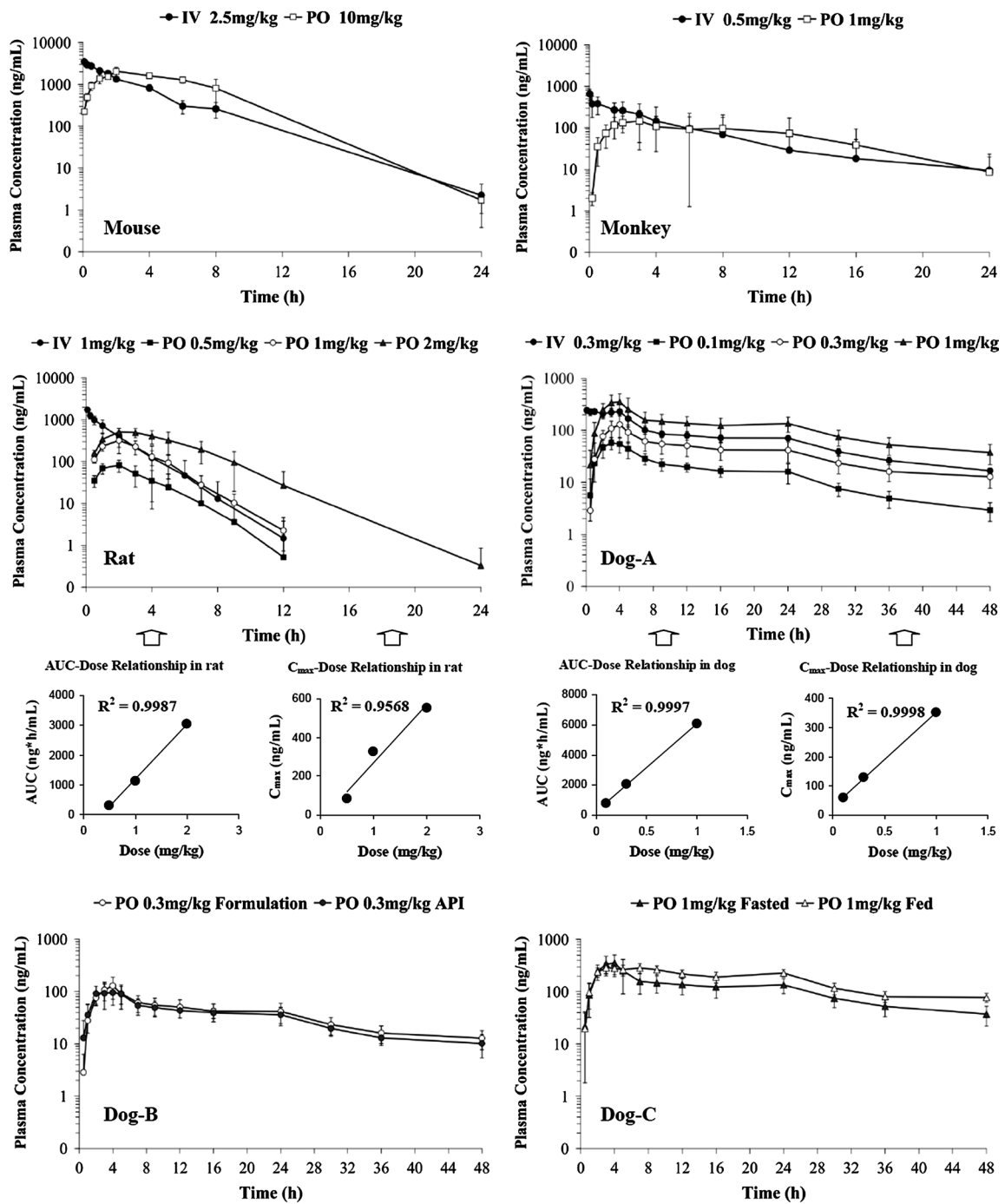


**Fig. 1** Mean plasma concentration–time profiles of HMPL-013 after single intravenous and oral administrations in mouse, rat, dog and monkey. Active pharmaceutical ingredient (API) was used in mouse, rat and monkey studies with suspension as the oral dosing formulation. In dog studies, *Dog-A* API was used for intravenous dosing, vet-

erinary capsule containing formulated ingredient was used for oral dosing; *Dog-B* API parallelly compared with formulated ingredient, both in veterinary capsule; *Dog-C* Self-controlled food effect comparison, formulated ingredient in veterinary capsule. Except in Plot *Dog-C*, all the dosing was conducted under fasted condition

of hepatic clearance. Comparing with the corresponding in vivo systemic clearance ( $CL_{sys}$ ) obtained after IV dosing, the  $CL_{hep, pred}$  is generally well consistent to the  $CL_{sys}$  with difference  $\leq 3$ -fold except for male mouse whose difference was about fivefold, but this difference was highly supposed

to be related to the unestimated microsomal protein binding.  $CL_{hep, pred}$  shows the best correlation with  $CL_{sys}$  in dogs, which had the slowest metabolic rate and was the most similar species to human. FMO seemed only contribute to the metabolism in mouse.

**Table 2** Statistical analysis results of major pharmacokinetic parameters of active pharmaceutical ingredient (API) versus formulation and fasted condition versus fed condition in dog pharmacokinetic studies of HMPL-013 ( $n = 6$ )

	API versus formulation			Fasted condition versus fed condition		
	$T_{\max}$	$C_{\max}$	$AUC_{\text{inf}}$	$T_{\max}$	$C_{\max}$	$AUC_{\text{inf}}$
<i>P</i> value	0.065	0.411	0.488	0.713	0.673	0.119

$T_{\max}$  Wilcoxon signed rank test

$C_{\max}$  and  $AUC_{\text{inf}}$  student *t* test after Log transformation

### Exploratory in vitro and in vivo MID, in vitro metabolite species comparison and human CYP reaction phenotyping

Three oxidative metabolites were identified in liver microsomes of all the species evaluated, as showed in Fig. 3. The structures of M1 (O-demethylation) and M2 (hydroxylation) were confirmed by the synthesized referenced compounds with corresponding company code as HM5013199 (M1) and HM5012569 (M2). M3 is a mono-oxidative metabolite whose exact structure is not elucidated yet. In general, the limited number of observed metabolites and the low relative abundance of the metabolites are consistent with the low turnover observed in metabolic stability studies with liver microsomes. As described in Fig. 4, species comparison indicated all of the human in vitro metabolites we have identified were found in the tested preclinical species, and dog was further proved to be the most similar species to human in terms of metabolite type, relative abundance and ranking. By using inhibitory monoclonal antibodies to individual CYP isoforms in human liver microsomes, CYP reaction phenotyping suggested multiple CYP isoforms were involved in the in vitro metabolism of HMPL-013 (Fig. 3; Table 6).

The exploratory in vivo MID in rat is summarized in Table 7. Similar to the in vitro metabolism, the major metabolic reaction in vivo was also demethylation and hydroxylation followed by the possible sequential metabolism including di-demethylation, demethylation plus hydroxylation and further glucuronide conjugation. No direct glucuronide conjugate of HMPL-013 was found. A little *N*-oxidation metabolite was found in plasma, but the relative abundance was minor. Bile had more metabolites than other tested matrices. Overall speaking, no special unpredictable metabolite was found in vivo compared with the in vitro findings.

### CYP inhibition and CYP induction potential

For the reversible CYP inhibition, all positive inhibitors showed potent inhibition to the relevant target CYP isoforms (maximal  $IC_{50} < 3.7 \mu\text{M}$ , data not shown). However, HMPL-013 exhibited no reversible inhibition potential to all tested CYP isoforms with  $IC_{50}$  all greater than  $50 \mu\text{M}$ .

Regarding to the time-dependent CYP inhibition, furaflyline ( $1 \mu\text{M}$ ) and azamulin ( $0.5 \mu\text{M}$ ) caused 80.5 and 85.1 % activity loss toward CYP1A2 and 3A4, respectively, when pre-incubated with human liver microsomes in presence of NADPH, suggesting a reliable system. However, HMPL-013 ( $10 \mu\text{M}$ ) caused no more than 27 % activity loss toward all tested CYP isoforms.

The induction fold of HMPL-013 ( $10 \mu\text{M}$ ) on the hPXR-mediated CYP3A4 transactivation against negative control was  $210 \pm 22 \%$ ; in contrast, the induction folds of rifampicin ( $10 \mu\text{M}$ ) and ritonavir ( $10 \mu\text{M}$ ) were  $350 \pm 32$  and  $550 \pm 64 \%$ , respectively. HMPL-013 ( $10 \mu\text{M}$ ) showed the induction folds of  $152 \pm 17$  and  $94 \pm 6 \%$  toward CYP1A2 and 3A4 in human hepatocytes, respectively, while omeprazole ( $10 \mu\text{M}$ ) showed induction fold of  $2,006 \pm 42 \%$  toward CYP1A2 and rifampicin ( $10 \mu\text{M}$ )  $1,012 \pm 42 \%$  toward CYP3A4. Thus, the CYP induction potential by HMPL-013 is negligible.

### Excretion

The major purpose of excretion study was to calculate the  $CL_{\text{R}}$  and  $CL_{\text{B}}$  of the unchanged HMPL-013 in rats. For these calculations, the excreted amount of parent drug without glucuronidase enzymolysis was used, although enzymolysis did not affect the amount of the unchanged HMPL-013.  $CL_{\text{R}}$  is about  $0.0037 \pm 0.0005 \text{ mL/min/kg}$  and  $CL_{\text{B}}$   $0.0210 \pm 0.0099 \text{ mL/min/kg}$ . Both are very small values, indicating in rats direct renal and biliary excretion of HMPL-013 is negligible.

In contrast to the unchanged HMPL-013 in urine and bile that was not affected by glucuronidase enzymolysis, the amount of M1 and M2 in urine and bile increased remarkably after enzymolysis. However, fecal excretion results were almost identical with or without glucuronidase enzymolysis. This observation was consistent with the in vivo MID results in rats (Table 7) that no direct HMPL-013 glucuronide conjugate was found, but sequential glucuronide conjugates were found as major metabolites in urine and bile but not found in feces. Thus, the feces results without enzymolysis and urine/bile results after enzymolysis are presented here. With the quantification of HMPL-013, M1 and M2 by the reference standards,

**Table 3** The bi-directional transport permeability and the efflux ratio of HMPL-013 across Caco-2 cell monolayers. HMPL-013 was evaluated at concentrations from 0.5 to 5  $\mu\text{M}$  and transport time from 60 to 120 min

	Substrate concentration ( $\mu\text{M}$ )	Incubation time (min)	$P_{\text{app}}$ ( $\times 10^{-6}$ cm/s)		Efflux ratio
			A–B <sup>c</sup>	B–A <sup>c</sup>	
Digoxin <sup>a</sup>	10	60	0.7	11.5	16.8
Digoxin + 10 $\mu\text{M}$ verapamil <sup>b</sup>			3.8	7.0	1.8
HMPL-013	1	60	32.8	35.1	1.1
HMPL-013 + 10 $\mu\text{M}$ verapamil			38.2	28.1	0.7
HMPL-013	0.5	60	30.3	37.5	1.2
	5		36.3	36.4	1.0
	1	90	30.7	34.0	1.1
		120	29.8	35.7	1.2

<sup>a</sup> Positive control as typical *P*-glycoprotein substrate with low permeability

<sup>b</sup> Typical efflux transporter inhibitor

<sup>c</sup> A–B: apical side to basolateral side; B–A: basolateral side to apical side

**Table 4** The binding fractions of HMPL-013 to plasma proteins in different species

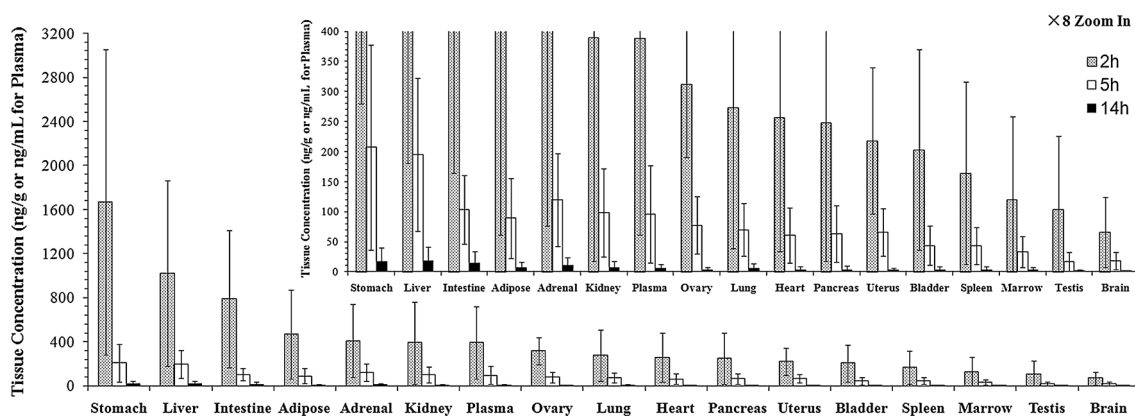
	Concentration ( $\mu\text{M}$ )	Binding fractions to plasma proteins (%)			
		Nude mouse	Rat	Dog	Human
HMPL-013	1	91.2	96.2	87.3	95.4
	3	92.7	95.6	88.7	95.3
	10	92.8	96.5	88.2	95.3
Hydrocortisone	5				48.8 <sup>a</sup>
Ketoconazole	5				98.0 <sup>b</sup>

<sup>a</sup> Reference data: 57 % [33]

<sup>b</sup> Reference data: 95 % [34]

the time-dependent excretion results (CER) are showed in Fig. 5. After 72 h post-dosing in non-BDC (bile duct-cannulated) rats, 22.1 % of the dose was recovered in feces in the forms of parent drug (10.4 %), M1 (9.7 %) and M2

(2.1 %); and 11.1 % of the dose was recovered in urine with 11.0 % as the form of M1 plus its potential glucuronide conjugates. Therefore, as a preliminary evaluation, currently the elimination pathways that had been clearly elucidated totally account for 33 % of the overall mass balance. It should be noted this is a preliminary study with cold compound and limited available metabolite standards, so evaluation of the dose recovery is a minor purpose and the results are only for reference. Both fecal and urinary excretion with currently known mechanism reached the maximum after 24 h post-dosing, indicating a low risk of undesirable prolonged retention or accumulation. In a separated study with BDC rats, 47.9 % of the dose was recovered in bile with 47.2 % as the form of M1 plus its potential glucuronide conjugates, after 24 h post-dosing. This result suggested metabolism to M1 and its potential glucuronide conjugates followed by biliary excretion was a main elimination pathway for HMPL-013 in rats at the tested dose.

**Fig. 2** Tissue distribution profiles of HMPL-013 in rats at 2, 5 and 14 h after oral administration of 1 mg/kg ( $n = 6$ )



**Table 5** The in vitro intrinsic clearance and scaled hepatic clearance of HMPL-013 from the liver microsomal incubations, compared with the in vivo systemic clearance after intravenous administration

Species	FMO contribution	Male			Female		
		CL <sub>int</sub> (mL/min/kg)	CL <sub>hep,pred</sub> (mL/min/kg)	CL <sub>sys</sub> (mL/min/kg)	CL <sub>int</sub> (mL/min/kg)	CL <sub>hep,pred</sub> (mL/min/kg)	CL <sub>sys</sub> (mL/min/kg)
Human	Normal	0.3	0.3	NA	2.1	1.9	NA
	FMO deactivation	0.6	0.6		2.1	1.9	
Monkey	Normal	36.9	20.1	8.7	NA	NA	6.9
	FMO deactivation	26.0	16.4		NA	NA	
Dog	Normal	1.8	1.7	1.5	0.8	0.8	1.2
	FMO deactivation	0.3	0.3		1.5	1.4	
Rat	Normal	21.6	16.5	10.0	25.2	18.5	6.0
	FMO deactivation	22.2	16.9		23.6	17.6	
Mouse	Normal	20.2	16.5	3.3	15.3	13.1	NA
	FMO deactivation	1.4	1.4		6.2	5.8	

CL<sub>int</sub> in vitro intrinsic clearance; CL<sub>hep,pred</sub> predicted hepatic clearance, based on a well-stirred model with no correction for potential protein binding and an assumption that oxidative metabolism was the major mechanism of hepatic clearance [14–16]. CL<sub>sys</sub>: in vivo systemic clearance obtained after intravenous administration, also showed in Table 1. FMO: Flavin monooxygenase. The FMO deactivation was achieved by heating the microsomes for 5 min in 45 °C water bath. NA not available

### Human PK prediction

By allometric scaling, CL<sub>u</sub> and V<sub>z,u</sub> of different species followed the equations as: CL<sub>u</sub> × MLP = 1.55 × BW<sup>0.74</sup>, V<sub>z,u</sub> = 1.14 × BW<sup>1.05</sup>. It was noted for CL<sub>u</sub>, the correction of maximal life span potential (MLP) was applied according to the RoE [19]. The V<sub>z,u</sub> and MLP-multiplied CL<sub>u</sub> showed excellent correlation with BW with the corresponding correlation coefficient r being 0.9958 and 0.9561, respectively. Therefore, it was reasonable to extend this relationship with human. After f<sub>u</sub> correction, the CL and V<sub>z</sub> in human were predicted to be 0.2 mL/min/kg and 0.8 L/kg.

The population PK modeling of the C-T data from individual dogs orally receiving formulated ingredient under fasted condition at 0.1, 3 and 1 mg/kg indicated a two-compartment oral PK model incorporating lag time (Tlag) with a multiplicative residual error model showing the best performance. The population means of absorption rate constant (Ka) and Tlag were 0.5342 h<sup>-1</sup> and 0.3671 h. The population means of Ka and Tlag were assumed to be equivalent to those of the human in the following simulation.

The simulated human PK profile after oral administration of HMPL-013 at 1 mg is illustrated in Fig. 6, comparing with the observed data in the FIH study with the same dose. It shows the simulated C-T curve is overall very well consistent with the observed data, especially for the terminal phase. The predicted FIH PK parameters were also compared with the actual data, as listed in Table 8. Except for the T<sub>max</sub> whose deviation fold is 4, all the predicted PK parameters are in excellent agreement with the actual data, with the deviation fold between 0.7 and 1.3. These results

suggest the considerable success of the human PK prediction. Upon this success, human minimal efficacious oral dose was predicted to be 3 mg, based on the AUC achieving the minimal efficacy in nude mice bearing BGC-823 xenograft and by the correction of corresponding species' f<sub>u</sub>.

### Discussion

Fruquintinib (HMPL-013) is a novel, potent, and selective small molecule VEGFR inhibitor developed as an orally available drug for the treatment of human cancers. In the present studies, the preclinical PK and ADME properties of HMPL-013 were characterized and its potential human PK profiles were assessed.

HMPL-013 has high intrinsic membrane permeability as showed in Caco-2 study, which is in accordance with its low polarity (very weak base with calculated pKa around 4.7) and moderate to high lipophilicity (logP around 2.9). No efflux was observed during the Caco-2 transport of HMPL-013 even at low concentrations. Therefore, efflux transporters would not limit its absorption considering the higher luminal substrate concentration during the absorption. These absorption properties, together with the low clearance, lead to good oral absorption in all tested preclinical species, as high exposure can be achieved at relatively low oral doses. Regarding to the dog oral PK modeling, it seemed incorporating Tlag at 0.3671 h (about 22 min) resulted in a better model. It is reasonable considering the poor solubility of HMPL-013 (0.55 µg/mL in pH7.4 buffer) and non-fully optimized solid formulation used in dog PK at early stage. Despite this, the model parameter Ka still

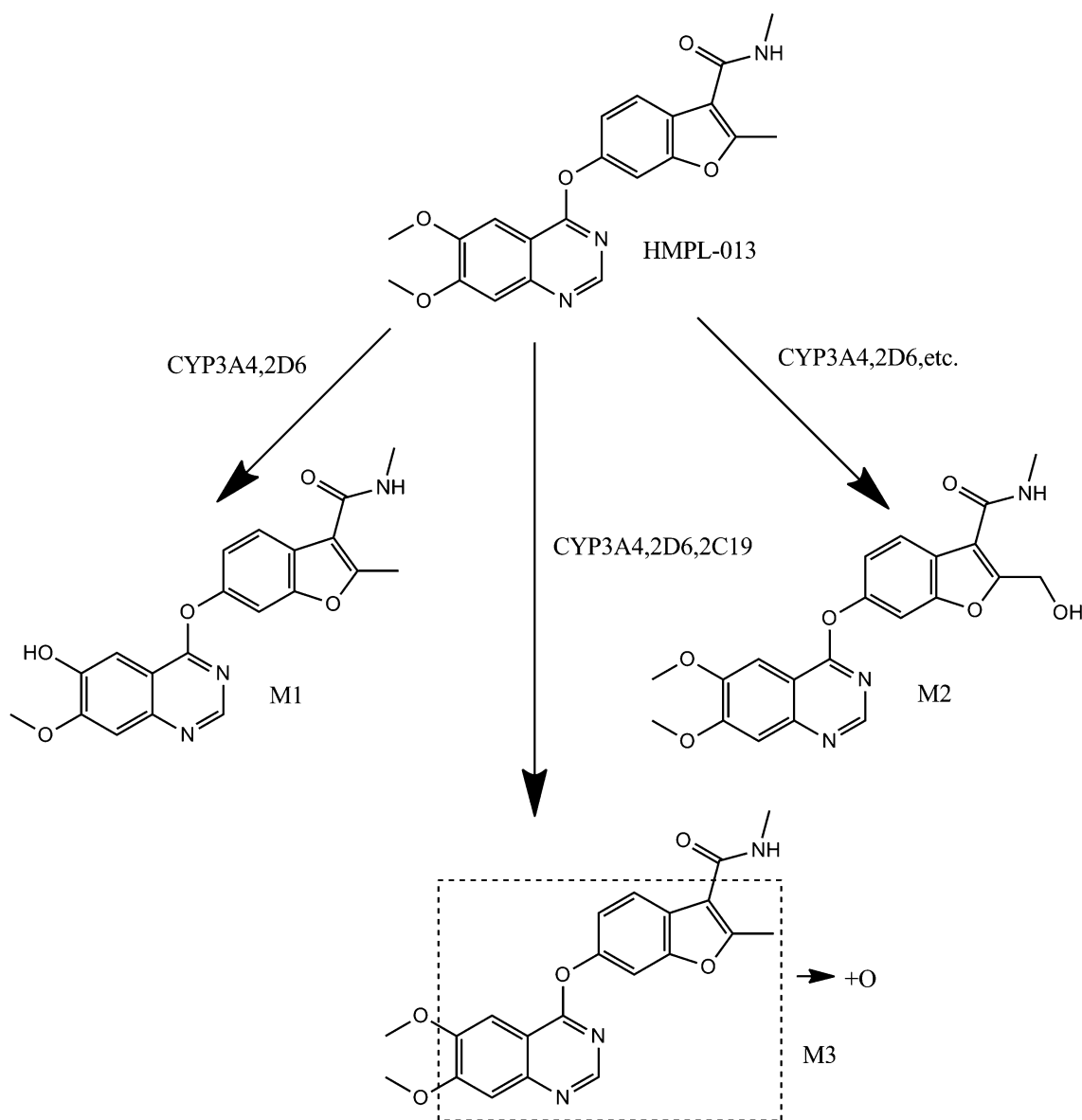


**Fig. 3** Proposed metabolic pathway of HMPL-013 in liver microsomes of mouse, rat, dog, monkey and human, with the contribution of cytochrome P450 enzymes to the metabolite formation in human liver microsomes

strongly suggests a rapid oral absorption, if looking  $K_a$  as the fractional rate of absorption which indicates more than 53 % of that in the absorption compartment was disappeared per hour (if neglecting the loss, most is absorbed) [23]. The  $T_{max}$  ranging from around 2–4 h in all tested species also indicates a rapid oral absorption. The good absorption is also reflected by the bioavailability, which is around 40–50 % in all tested species and shows the remarkable minimal species difference. This implicates the low risk of variation in human oral absorption. Food seems to have no statistically meaningful effect on the absorption in dogs, despite the specious trend of higher absorption after feeding. This is possibly due to the high permeability of

HMPL-013 bypassing its low solubility, and this may further lower the risk of variation in human absorption. So overall, these good absorption properties support HMPL-013 to be developed as an orally given drug.

The  $V_z$  of HMPL-013 suggests a moderate to high volume of distribution, as the largest  $V_z$  observed in monkey is about fivefold of the total body water volume. This is a favorable property, since it implicates the substantial extravascular tissue distribution which can facilitate the target accessibility, and in contrast, the low risk of excessive tissue binding, which may lead to undesirable toxicity, if recalling  $V_z$  reflects the competitive relationship between plasma binding and tissue binding [24] and considering

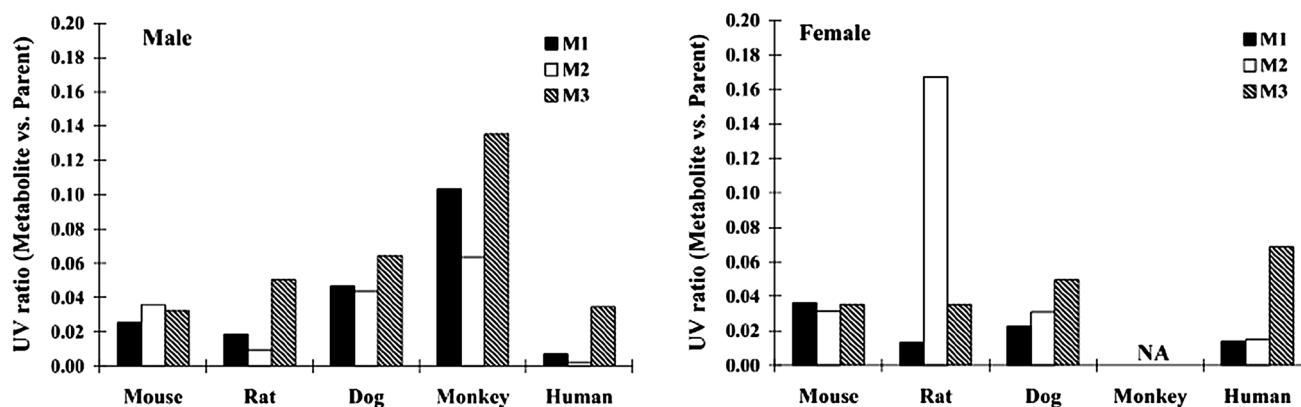


**Fig. 4** Species comparison of in vitro metabolites in liver microsomes of mouse, rat, dog, monkey and human. Relative abundance was expressed as peak area ratios of metabolite to parent compound

obtained in UV detection. Female monkey microsomes were unavailable at the time of experiment

**Table 6** The contribution of cytochrome P450 (CYP) isoenzymes to the formation of three HMPL-013 in vitro metabolites in human liver microsomes (CYP reaction phenotyping with monoclonal antibody)

	1A2 (%)	2A6	2B6	2C8 (%)	2C19 (%)	2E1	2D6 (%)	3A4 (%)
<i>Relative metabolite formation percentage<sup>a</sup></i>								
Positive controls <sup>b</sup>	16.6	–	–	19.8	7.7	–	15.5	15.8
M1	97.1	117.5 %	115.5 %	80.5	88.1	99.5 %	65.8	35.2
M2	112.4	126.0 %	119.7 %	80.7	84.7	103.1 %	79.4	71.9
M3	105.9	120.4 %	130.7 %	83.6	76.2	102.0 %	72.1	16.5

<sup>a</sup> Antibody treatment versus no antibody treatment

<sup>b</sup> Acetaminophen formation from phenacetin for 1A2; 6 $\alpha$ -hydroxypaclitaxel formation from paclitaxel for 2C8; 4'-hydroxymephenytoin formation from S-mephenytoin for 2C19; dextrophan formation from dextromethorphan for 2D6; 6 $\beta$ -hydroxytestosterone formation from testosterone for 3A4

HMPL-013 also has moderately high plasma protein binding. Tissue distribution in vivo studied in rats partially proved this interpretation, as HMPL-013 was widely distributed to most organs with the similar pattern as plasma and there was no specific tissue accumulation. The highest distribution in GI tract and liver is well correlated with its oral dosing. The relatively high distribution to adipose agrees with its lipophilicity. The lowest distribution in brain, bone marrow and testis indicates HMPL-013 can hardly pass through the well-organized barriers. Considering its lipophilicity and membrane permeability, the reason needs to be further investigated. Although HMPL-013 showed no efflux in Caco-2 study, being the substrate of some unknown efflux transporters can not be excluded given the different nature between Caco-2 monolayers and blood–brain or blood–testis barriers.

Regarding to elimination, including metabolism and excretion, HMPL-013 is proved to be a low-cleared compound in all tested preclinical species based on the ranking of the extent of either hepatic extraction or body extraction, with phase I metabolism accounting for its major

elimination. Firstly, the  $CL_{\text{hep,pred}}$  from in vitro metabolic stability is generally well consistent to the  $CL_{\text{sys}}$  observed in vivo in all tested preclinical species. As  $CL_{\text{hep,pred}}$  scaling was based on the assumption that oxidative metabolism predominated the hepatic clearance, so this consistency implicates the validity of the assumption and the potential exclusion of the direct excretion and the direct phase II conjugation. Secondly, both the in vivo MID and excretion study in rats did not find any direct phase II conjugates of HMPL-013, which supports the exclusion of direct phase II conjugation. Finally, the excretion study reveals the  $CL_{\text{R}}$  and  $CL_{\text{B}}$  of the unchanged HMPL-013 in rats are significantly low, which further supports the exclusion of direct urinary or biliary excretion. Dividing the  $CL_{\text{R}}$  by the total plasma clearance CL in rats, the fraction excreted ( $f_{\text{e}}$ ) of HMPL-013 is estimated as 0.05 %, resulting in the fraction metabolized ( $f_{\text{m}}$ ) of HMPL-013 higher than 99 %. The  $CL_{\text{R}}$  of HMPL-013 in rats is around 50-fold lower than the product of corresponding  $f_{\text{u}} \times \text{GFR}$  (glomerular filtration rate) [20], indicating extensive tubular reabsorption [23]. Knowing HMPL-013 is a very weakly basic nonpolar compound

**Table 7** In vivo metabolite information of HMPL-013 in rats after oral administration at 1 mg/kg

	Bile	Urine	Feces	Plasma
Number of metabolites identified	13	7	8	9
Major metabolic reaction	Demethylation, hydroxylation, demethylation plus hydroxylation, di-demethylation, sequential glucuronide conjugation	Demethylation, hydroxylation, demethylation, sequential glucuronide conjugation	Demethylation, hydroxylation, di-demethylation,	Demethylation, hydroxylation, <i>N</i> -oxidation, sequential glucuronide conjugation

with calculated pKa around 4.7, it is understandable because virtually 100 % is un-ionized regardless of urine pH while tubular reabsorption of xenobiotics, in contrast to active secretion, is predominantly mediated by passive diffusion [23]. Elucidation of renal elimination mechanism preclinically is essential for the prediction of clinical pharmacology. Actually, as determined by the compound nature itself, similar renal elimination profiles were observed in clinic lately. In terms of  $CL_B$ , it is also much lower than the rat's bile flow [20], indicating parent HMPL-013 is not favored by biliary excretion.

Regarding to the metabolites, exploratory in vitro MID identified three metabolites in the phase I metabolism system in liver microsomes of different species. The metabolic reactions: *O*-demethylation, hydroxylation and oxidation were further confirmed in vivo in rats, with sequential metabolism happened. The general consistency of the MID results in vitro and in vivo and the common metabolic reactions suggests a low risk of unpredicted metabolic-related toxicity. The cross-species metabolite profiles suggest dog is the most similar to human, which agrees with the similarity of dog to human in terms of turnover rate. This information supports the selection of dog and rat for the further toxicological evaluation, also recalling rat is most similar to human in terms of plasma protein binding.

As the chemical standards of M1 (*O*-demethylation) and M2 (hydroxylation) were available, they were used in the rat excretion study. After 72 h post-dosing in non-BDC rats, 33 % of the dose can be recovered as the related materials of parent compound, M1 and M2. Remember that mass balance recovery was not the main purpose of current excretion study, which was conducted with the cold compound and limited metabolite standards. The fate of the remaining 67 % of dose needs to be further investigated. However, upon the current knowledge, oxidative metabolism to M1 with sequential glucuronidation followed by both biliary and urinary excretion is a very important elimination mechanism for HMPL-013. Moreover, based on the biliary excretion results in BDC rats and the fact that most metabolites were identified in bile, biliary excretion of drug-related materials seems more important for HMPL-013 than urinary excretion. Comparing the biliary excretion results in BDC rats to the fecal excretion results in non-BDC rats, enterohepatic circulation is suspected, which can also be speculated from the "plateau phase" in the PK profiles of species with cholecyst [25], and is interestingly not observed in rats.

Although M1 was found an important metabolite in vitro and in vivo, its VEGFR inhibition activity is more than 20-fold higher than the parent drug. Therefore, the target-related effect arising from M1 is less important, and the systemic exposures of M1 were not measured in the current in vivo PK studies.

**Fig. 5** The cumulative excretion rate (CER, maximum 100 %) of HMPL-013, in the forms of parent drug (P), M1 and M2, after oral administration at 1 mg/kg to SD rats. Feces and urine were harvested in one study with non-BDC (bile duct-cannulated) rats, while bile was collected in a separated study with BDC rats. Feces results: without glucuronidase enzymolysis; urine and bile results: with glucuronidase enzymolysis

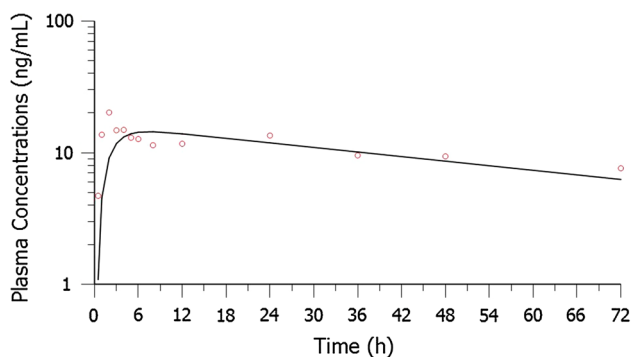
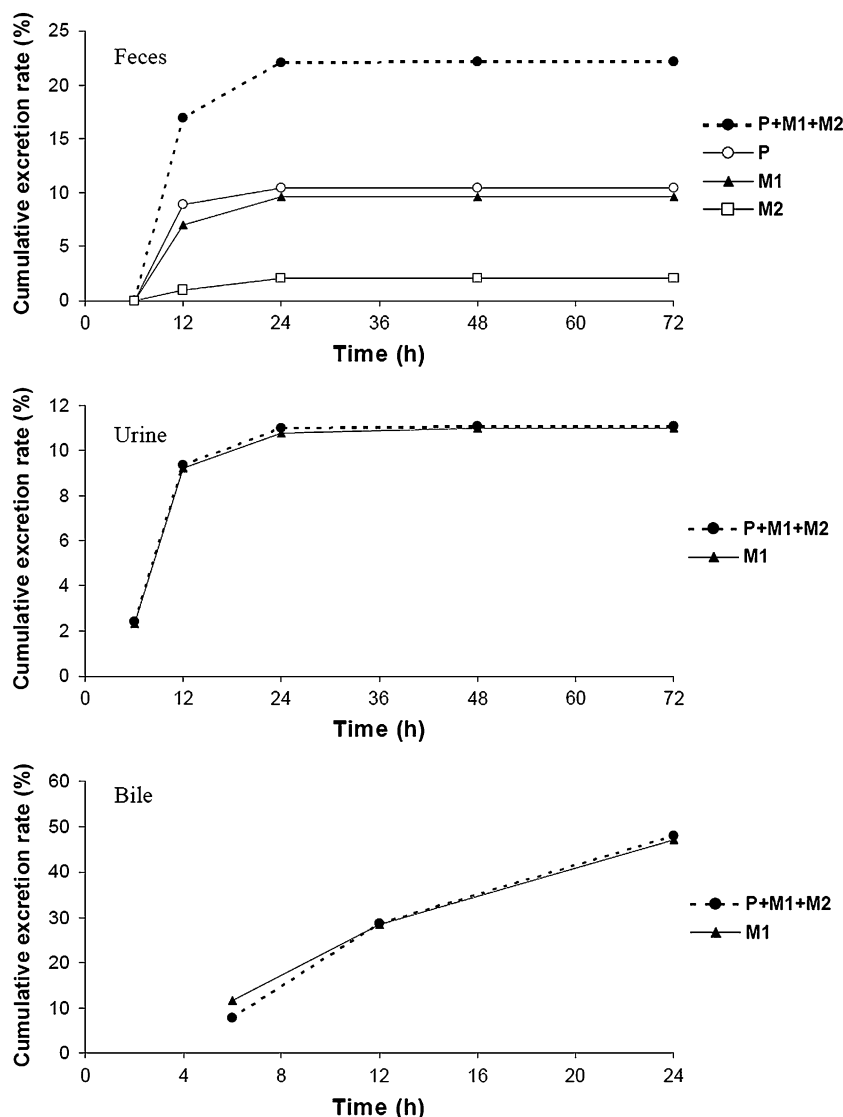


**Fig. 6** The simulated plasma concentration versus time profile of HMPL-013 in human after oral administration at 1 mg (line), compared with the observed plasma concentration data (circle dot) from the first-in-human study with the same oral dose

Regarding to the pharmacokinetic DDI, the most important issue is the CYP-related metabolism-based DDI. HMPL-013 shows neither reversible nor time-dependent inhibition on the major human CYP isoforms in liver microsomes. It also has no induction potential on CYP1A2 and 3A4 in human hepatocytes, and no activation of hPXR which controls the expression of 3A4. Thus, HMPL-013 has minimal risk to be a CYP perpetrator in clinic. On the other hand, in current preliminary reaction phenotyping with human CYPs, M1 formation is mainly mediated by 3A4 with 2D6 stands second; 3A4 plays the predominant role in M3 formation with 2C19 and 2D6 contributing a little; it remains ambiguous for the contribution of 2D6 and 3A4 to the formation of M2 if using 80 % as a cut-off. So whether other enzymes than currently tested CYPs



**Table 8** The predicted human PK parameters of HMPL-013 after oral administration at 1 mg generated based on the simulated plasma concentration versus time data, compared with the actual PK param-

eters calculated based on the observed plasma concentration versus time data in the first-in-human study with the same oral dose

	$\lambda_z$ (1/h)	$T_{1/2}$ (h)	$T_{max}$ (h)	$C_{max}$ (ng/mL)	$AUC_{0-72h}$ (h*ng/mL)	$AUC_{inf}$ (h*ng/mL)	$V_z/F$ (L)	CL/F (mL/min)	$MRT_{inf}$ (h)
Observed	0.01064	65.1	2	20.2	759	1,450	64.8	11.5	95.9
Predicted	0.01330	52.1	8	14.4	722	1,193	63.0	14.0	77.1
Deviation fold	1.3	0.8	4.0	0.7	1.0	0.8	1.0	1.2	0.8

Deviation fold = predicted value/observed value

involving in the M2 formation needs further investigation. Anyway, it is clear that multiple enzymes are involved in HMPL-013 metabolism. So the risk to be a CYP victim in clinic is also low for HMPL-013. Not activating hPXR also indicates HMPL-013 will probably not induce some transporters, like *P-gp*, after multi-dosing. Alteration in plasma binding is traditionally but misleadingly regarded as a source of clinical DDI [26]. As an oral-administration drug with predominant hepatic clearance and low extraction ratio, changes in plasma protein binding of HMPL-013 has no clinical relevance [27]. Besides, binding of HMPL-013 to plasma proteins keeps linear in a large concentration range up to 10  $\mu$ M, in contrast to the predicted low human dose and the consequent low human plasma concentrations. So overall, the pharmacokinetic DDI risk for HMPL-013 is low.

Human primary PK parameters were predicted by an empirical approach using allometry with mouse, rat and dog after  $f_u$  correction, in order to assess the viability of HMPL-013 being a clinical drug candidate. The exclusion of monkey in the presented allometry is due to the lack of monkey  $f_u$  and the poor predictability when incorporating cynomolgus. To our knowledge and experiences, cynomolgus monkey is generally likely to be the outlier for human PK prediction. Actually, allometric scaling was also done by incorporating monkey and without  $f_u$  correction. However, the presented method with cynomolgus excluded and  $f_u$  correction demonstrates the best predictability. Correction by  $f_u$ , which is based on the “free-drug hypothesis” [28], seems more close to the real situation and can significantly improve the prediction. Human CL was predicted with the MLP correction. The predicted human CL by allometry is 0.2 mL/min/kg. In addition, assuming human CL is predominated by the hepatic clearance as reflected in rats, which can be estimated by in vitro scaling using human liver microsomes, human CL is about 1.1 mL/min/kg (the average of male and female results). This value is only around fivefold biased to the allometric value, which is still within the acceptable range of prediction variability. So overall, HMPL-013 tends to have a very low clearance extent in human.  $V_z$  typically correlates well with the BW and therefore was predicted by simple allometric scaling.

The predicted human  $V_z$  is higher than total body water volume [20] with 0.8 L/kg suggesting HMPL-013 distributes to tissues. Upon CL and  $V_z$ , the predicted long  $t_{1/2}$  (about 50 h) in human supports once a day dosing, while implicates a long time (around 10 days) to reach the steady state. This dose regime, in combination with the long  $t_{1/2}$ , can result in a favorable minimal concentration fluctuation at steady state, though there will be a threefold to fourfold steady state accumulation, according to linear PK principles [29]. Once daily dosing also increases the patient compliance.

The prediction of human PK profile by simulation based on a one-compartment model fortunately achieved considerable success. Especially, the consistency of terminal phase suggests a highly successful prediction of CL and  $V_z$ . Although physiological based PK (PBPK) modeling has been widely advocated and applied in human PK prediction [30], allometric scaling still remains significant utility, as it is enough straightforward, easy to handle for non-modeler and has even better prediction in particular situations sometimes. However, prediction of human oral absorption profile of HMPL-013 seems relatively poor as reflected by the inconsistency of the early phase. While this problem still remains a big challenge for general human absorption prediction [31]. Here we used the model parameters generated from dog’s oral absorption with solid formulation to substitute for the human’s, which is commonly used in industry at the early stage. But this approach is too much empirical. It is necessary to try the more physiologically based “ACAT model” [32] to improve the human absorption prediction of HMPL-013 from mechanistic standpoint, when more physiochemical parameters of the human formulation are obtained. It should be pointed out that as there were three dose levels in dog oral PK, population method was used to simultaneously model the data from all the dose levels, which could not be achieved by classic PK modeling, in order to capture the more typical population means from larger sample size to better reflect the overall absorption behaviors.

The human minimal efficacious oral dose was projected using a simple PK equation linking the dose with CL and AUC, also considering the “free-drug hypothesis” [28].

Although the projected dose is reasonable, it is necessary to further conduct the PK/PD modeling for better understanding of the mechanistic relationships and therefore to better predict the dose regimen in further clinical trials.

The most drawbacks of the current studies is that the comprehensive tissue distribution and mass balance, together with the more predominant elimination pathway, of HMPL-013 are not elucidated clear enough. But this can be resolved by doing radiolabeled studies firstly in animals then in human, which is generally planned after proof of concept in clinic.

## Conclusion

Fruquintinib (HMPL-013) exhibits favorable preclinical PK properties with low clearance, good oral exposures with dose dependency, favorable tissue distribution extent and low clinical DDI potential. Human PK parameters and profiles, predicted by empirical methods, all show favorable properties. The projected human minimal efficacious dose is also reasonable. The overall promising results warrant further investigation for its therapeutic potential in human.

**Acknowledgments** The authors are sincerely thankful for the great contributions of Prof. Dafang Zhong and Prof. Xiaoyan Chen from Shanghai Institute of Materia Medica to the rat and dog's studies, Prof. Zhuohan Hu from Research Institute for Liver Diseases (Shanghai) Co. Ltd. to the human hepatocyte study and Dr. Renke Dai from Zhongshan PharmaSS Corporation to the hPXR study. Appreciations are also given to all the colleagues in Hutchison MediPharma who contributed to the HMPL-013 project.

**Conflict of interest** The authors were all employees of Hutchison MediPharma Limited when the study was conducted and are alone responsible for the content and writing of this paper.

## References

- Mendel DB, Laird AD, Xin X, Louie SG, Christensen JG, Li G, Schreck RE, Abrams TJ, Ngai TJ, Lee LB (2003) In vivo anti-tumor activity of SU11248, a novel tyrosine kinase inhibitor targeting vascular endothelial growth factor and platelet-derived growth factor receptors. *Clin Cancer Res* 9:327–337
- Ferrara N (2002) VEGF and the quest for tumour angiogenesis factors. *Nat Rev Cancer* 2:795–803
- Wedge SR, Kendrew J, Hennequin LF, Valentine PJ, Barry ST, Brave SR, Smith NR, James NH, Dukes M, Curwen JO (2005) AZD2171: a highly potent, orally bioavailable, vascular endothelial growth factor receptor-2 tyrosine kinase inhibitor for the treatment of cancer. *Cancer Res* 65:4389–4400
- Morabito A, De Maio E, Di Maio M, Normanno N, Perrone F (2006) Tyrosine kinase inhibitors of vascular endothelial growth factor receptors in clinical trials: current status and future directions. *Oncologist* 11:753–764
- Cook KM, Figg WD (2010) Angiogenesis inhibitors: current strategies and future prospects. *CA Cancer J Clin* 60:222–243
- Chow LQM, Eckhardt SG (2007) Sunitinib: from rational design to clinical efficacy. *J Clin Oncol* 25:884–896
- Iyer R, Fetterly G, Lugade A, Thanavala Y (2010) Sorafenib: a clinical and pharmacologic review. *Expert Opin Pharmacother* 11:1943–1955
- Bhargava P, Robinson MO (2011) Development of second-generation VEGFR tyrosine kinase inhibitors: current status. *Curr Oncol Rep* 13:103–111
- Azmi AS, Wang Z, Philip PA, Mohammad RM, Sarkar FH (2010) Proof of concept: network and systems biology approaches aid in the discovery of potent anticancer drug combinations. *Mol Cancer Ther* 9:3137–3144
- Hellström M, Gerhardt H, Kalén M, Li X, Eriksson U, Wolburg H, Betsholtz C (2001) Lack of pericytes leads to endothelial hyperplasia and abnormal vascular morphogenesis. *J Cell Biol* 153:543–553
- Hu-Lowe DD, Zou HY, Grazzini ML, Hallin ME, Wickman GR, Amundson K, Chen JH, Rewolinski DA, Yamazaki S, Wu EY (2008) Nonclinical antiangiogenesis and antitumor activities of axitinib (AG-013736), an oral, potent, and selective inhibitor of vascular endothelial growth factor receptor tyrosine kinases 1, 2, 3. *Clin Cancer Res* 14:7272–7283
- Patson B, Cohen BR, Olszanski AJ (2012) Pharmacokinetic evaluation of axitinib. *Expert Opin Drug Metab Toxicol* 8:259–270
- Gu Y, Wang GJ, Wu XL, Zheng YT, Zhang JW, Ai H, Sun JG, Jia YW (2010) Intestinal absorption mechanisms of ginsenoside Rh2: stereoselectivity and involvement of ABC transporters. *Xenobiotica* 40:602–612
- Kuhn W, Gieschen H (1998) Predicting the oral bioavailability of 19-nortestosterone progestins in vivo from their metabolic stability in human liver microsomal preparations in vitro. *Drug Metab Dispos* 26:1120–1127
- Obach RS (1999) Prediction of human clearance of twenty-nine drugs from hepatic microsomal intrinsic clearance data: an examination of in vitro half-life approach and nonspecific binding to microsomes. *Drug Metab Dispos* 27:1350–1359
- Obach RS, Baxter JG, Liston TE, Silber BM, Jones BC, Macintyre F, Rance DJ, Wastall P (1997) The prediction of human pharmacokinetic parameters from preclinical and in vitro metabolism data. *J Pharmacol Exp Ther* 283:46–58
- Center for Drug Evaluation and Research FaDA (2001) Guidance for industry: bioanalytical method validation
- Fura A, Vyas V, Humphreys W, Chimalokonda A, Rodrigues D (2008) Prediction of human oral pharmacokinetics using nonclinical data: examples involving four proprietary compounds. *Biopharm Drug Dispos* 29:455–468
- Mahmood I, Balian JD (1996) Interspecies scaling: predicting clearance of drugs in humans. Three different approaches. *Xenobiotica* 26:887–895
- Davies B, Morris T (1993) Physiological parameters in laboratory animals and humans. *Pharm Res* 10:1093–1095
- Wilkinson GR, Shand DG (1975) Commentary: a physiological approach to hepatic drug clearance. *Clin Pharmacol Ther* 18:377–390
- Toutain PL, Bousquet-Melou A (2004) Plasma clearance. *J Vet Pharmacol Ther* 27:415–425
- Rowland M, Tozer T (2011) Clinical pharmacokinetics and pharmacodynamics: concepts and application, 4th edn. Lippincott Williams & Wilkins, a Wolters Kluwer business, New York
- Toutain PL, Bousquet-Melou A (2004) Volumes of distribution. *J Vet Pharmacol Ther* 27:441–453
- Berezhkovskiy LM (2008) Prediction of the possibility of the second peak of drug plasma concentration time curve after iv bolus administration from the standpoint of the traditional multi-compartmental linear pharmacokinetics. *J Pharm Sci* 97:2385–2393

26. Rolan PE (1994) Plasma-protein binding displacement interactions—why are they still regarded as clinically important. *Br J Clin Pharmacol* 37:125–128
27. Benet LZ, Hoener BA (2002) Changes in plasma protein binding have little clinical relevance. *Clin Pharmacol Ther* 71:115–121
28. Tillement JP, Urien S, Chaumet-Riffaud P, Riant P, Bree F, Morin D, Albengres E, Barre J (1988) Blood binding and tissue uptake of drugs: recent advances and perspectives. *Fundam Clin Pharmacol* 2:223–238
29. Toutain PL, Bousquet-Melou A (2004) Plasma terminal half-life. *J Vet Pharmacol Ther* 27:427–439
30. Poulin P, Jones RDO, Jones HM, Gibson CR, Rowland M, Chien JY, Ring BJ, Adkison KK, Ku MS, He H, Vuppugalla R, Marathe P, Fischer V, Dutta S, Sinha VK, Bjornsson T, Lave T, Yates JWT (2011) PHRMA CPCDC initiative on predictive models of human pharmacokinetics, Part 5: prediction of plasma concentration-time profiles in human by using the physiologically-based pharmacokinetic modeling approach. *J Pharm Sci* 100:4127–4157
31. Rowland M, Peck C, Tucker G (2011) Physiologically-based pharmacokinetics in drug development and regulatory science. *Annu Rev Pharmacol Toxicol* 51:45–73
32. Huang W, Lee SL, Yu LX (2009) Mechanistic approaches to predicting oral drug absorption. *AAPS J* 11:217–224
33. Lee KJ, Mower R, Hollenbeck T, Castelo J, Johnson N, Gordon P, Sinko PJ, Holme K, Lee YH (2003) Modulation of nonspecific binding in ultrafiltration protein binding studies. *Pharm Res* 20:1015–1021
34. Niggebrugge AE, MacLauchlin C, Dai D, Ford LA, Menendez AT, Chilton AS (2002) A high throughput protein binding assay by cohesive turbulent flow liquid chromatography mass spectrometry to support drug discovery. In: The 50th ASMS conference on mass spectrometry and allied topics, Orlando, Florida